Radiation Budget over the Indian Monsoon Region

By
Tracy Lorraine Smith and Stephen K. Cox

Department of Atmospheric Science
Colorado State University
Fort Collins, Colorado

Colorado State University

Department of Atmospheric Science

Paper No. 376

RADIATION BUDGET OVER THE INDIAN MONSOON REGION

by

Tracy Lorraine Smith

and

Stephen K. Cox

Research supported by
The National Science Foundation
Grant No. ATM-8010691

Department of Atmospheric Science
Colorado State University
Fort Collins, Colorado

February, 1984

Atmospheric Science Paper Number 376

ABSTRACT

RADIATION BUDGET OVER THE INDIAN MONSOON REGION

A top of the atmosphere radiation budget is calculated over the Indian monsoon region for January, February, May, June, July and August of 1979 from data collected as a part of the monsoon experiment, MONEX. Albedos were inferred for 23 surface-type areas using GOES-1 satellite data in conjunction with equations derived from comparison of the satellite data with concurrent aircraft measurements. The longwave radiation values used in the budgets were monthly averages derived from the Nimbus-7 ERB experiment.

A regional minimum in albedo was found for the month of May, with a corresponding rise in albedo in June. The net radiation for May exhibited a positive (surplus) net radiation values over the entire study area, including the deserts. In June, a small region of local minimum values of net radiation developed over the west Indian coast and adjacent ocean areas. This area of relative low net values moved over the Indian subcontinent in July, and persisted through August. The study region as a whole was found to be a net radiative source region, with the contributions of areas with surpluses far outweighing the values for the deficit areas. Comparisons of this study with previous studies by Winston, 1971 and Winston and Krueger, 1977 show

good correlation between the subnormal monsoon year of 1976 and the study year, 1979, also considered to be subnormal in terms of precipitation amounts.

Tracy Lorraine Smith
Atmospheric Science Department
Colorado State University
Fort Collins, Colorado 80523
Fall, 1983

ACKNOWLEDGEMENTS

The author wishes to thank her advisor, Dr. Stephen K. Cox for his guidance and support. Gratitude is also extended to the members of the author's committee, Dr. Elmar Reiter and Dr. G. C. Wilken for their valuable advice. Special thanks are due to Melissa Tucker for her careful typing and general assistance with the manuscript; John Graffy for his programming assistance; John Davis, Steven Ackerman, Larry Freeman and David Randel for their discussions and information, and to Judy Sorbie for her drafting of the study area. My deepest gratitude and love to my husband, Scott Blunk, for his continual support and encouragement.

The study was supported by the National Science Foundation grant number ATM 8010691.

TABLE OF CONTENTS

I. INTRODUCTION

The Indian monsoon is a regional circulation with global impact. The word "monsoon" has been used in varying ways. One definition is "seasonal winds (derived from Arabic mausim, a season). It was first applied to the winds over the Arabian Sea, which blow for six months from northeast and for six months from southwest, but it has been extended to similar winds in other parts of the world... The primary cause is the much greater annual variation of temperature over large land areas compared with neighboring ocean surfaces, causing an excess of pressure over the continents in winter and a deficit in summer, but other factors such as the relief features of the land have a considerable effect." The Indian monsoon is an excellent example of this type of circulation. Although it is generally accepted that the difference in heating between the ocean and land areas is a major influence in the creation of the monsoon circulation (Ramage, pg. 8, 1971), the magnitudes of the actual heat budget components remain to be determined. The heat budget of an atmospheric system such as the Indian monsoon, ignoring horizontal and vertical transport, consists of balancing the effects of shortwave radiative and condensational heating with the effects of longwave radiative and evaporative cooling. Heat transfer in the atmosphere occurs in three ways: conduction, convection and radiation. Since conduction requires actual contact between the mediums involved in the energy exchange, it has a limited impact

on the vertical exchanges of energy through deep layers of the atmosphere. However, both convection and radiation are important mechanisms in redistributing heat vertically in the atmosphere. This can be illustrated by considering the monsoon region as a closed system, or "box" in the atmosphere. If one ignores advection from outside the system, radiation is the only incoming energy source. Within the box there are many forms of energy transfer occurring; conduction, condensation, vertical motion, and convection. The energy for all this activity enters through the "top" of the box, or in reality, the top of the atmosphere, in the form of radiation. Thus, knowledge of the radiation budget (solar radiation in, longwave radiation and reflected solar radiation out) is important in understanding the motions of the atmosphere by giving one a feeling for the energy available for these motions. This study is an attempt to ascertain the sign and magnitude of the radiation budget over the monsoon region in 1979, an area bounded (for this study) by 25°E to 92°E longitude and 5°S to 43°N latitude, and compare this budget to previous years.

I.A. The Indian Monsoon

In the winter months over the Indian subcontinent, the predominant surface wind flow is a weak movement of the dry air from the subcontinent to the surrounding ocean areas. This has been explained as the response of the atmosphere to the difference in temperature, and therefore pressure, between the cool land and the warm water, creating a giant "sea-breeze" effect over that part of the globe (Ramage, pg. 11, 1971). In a sea-breeze circulation, the air flows from high pressure over the cooler area to the relatively low pressure over the

warm area, whether the area is land or water. In the summer months, the situation reverses and the winds blow from the cooler ocean to warmer land, bringing moisture to the Indian subcontinent. This moisture is the lifeblood of Indian agriculture, and knowing when it will arrive and in what amount is an issue of vital importance to the Indian people.

The sea-breeze circulation is the basic circulation of the monsoon system. A monsoon would occur without any other meteorlogical influences, but in a much weaker form (Ramage, pg. 15, 1971). There are several major elements that develop in the Northern Hemispheric summer (June, July, and August) that act to intensify the monsoon circulation. These include the influence of the Tibetan Plateau, the low-level cross equatorial jet, and the monsoon trough. The Tibetan Plateau acts as a barrier between the Indian subcontinent and rest of the Asian land mass. This inhibits the exchange of air masses, resulting in an exaggerated N-S temperature gradient in the winter, and, since the plateau becomes a heat source in the summer, it decreases the N-S temperature gradient at latitudes between 20°N and 40°N from that which would otherwise be expected. Centered over the Plateau during the Northern Hemisphere summer is a large upper tropospheric anticyclone with its maximum intensity at 200 millibars (mb); this anticyclone is called the "Tibetan High" (Krishnamurti and Bhalme, 1976). This feature first develops in the upper troposphere in April, and is just to the north of Borneo. It then begins a three month migration, until by mid-June it has established itself over Tibet. It migrates back to the south in September and October, and is

insignificant thereafter. The progression of this feature can be seen in figures 1.1 and 1.2.

The low-level cross equatorial jet is an atmospheric response to oceanic temperature gradients arising from upwelling along the coasts of Somalia and Arabia (Ramage, 1971). The upwelling first appears in May, as the southwest monsoon winds develop and create shearing stress on the water along the coasts. As the water is pushed away from shore, colder water rising from beneath takes its place. This colder, upwelling water is further cooled by evaporation. The pool of cold water creates an area of relatively cool air above it in the western Arabian Sea, and this, in turn, causes the formation of the thermal jet (Bunker,1968). The location and characteristics of the jet in August are illustrated in figure 1.3. The magnitude of the cooling of the air is approximately ten times as much as over the rest of the Arabian Sea. The maximum winds are found at approximately 1.5 kilometers (km), and have been recorded at speeds of up to 100 m/s over Madagascar and the Somali coast.

The summer surface pressure trough over India, also known as the "monsoon trough", is oriented from NW to SE, roughly parallelling the Himalayas (fig. 1.4). The northern end is anchored in the heat low over Pakistan, and the southern end is in the cyclogenetic area of the Bay of Bengal. Its location is very likely influenced by the topography of the area (Flohn, 1968). Each of these phenomemon have a continuing effect on the monsoon circulation.

The transition from winter to summer monsoon flow takes place in the months of March and April. During this time the prevailing winds shift from NE to W or SW, while radiational heating has caused a heat

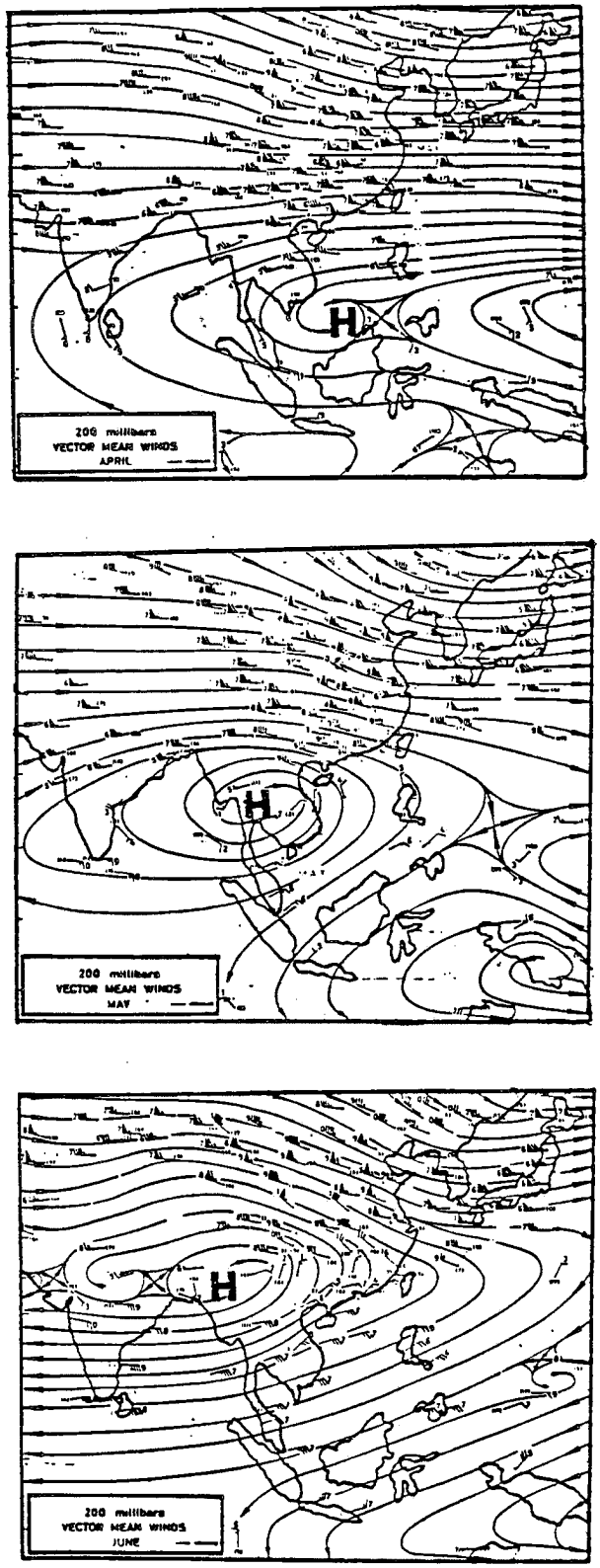

Figure 1.1. Movement of the Tibetan High, Krishnamurti and Bhalme, 1976.

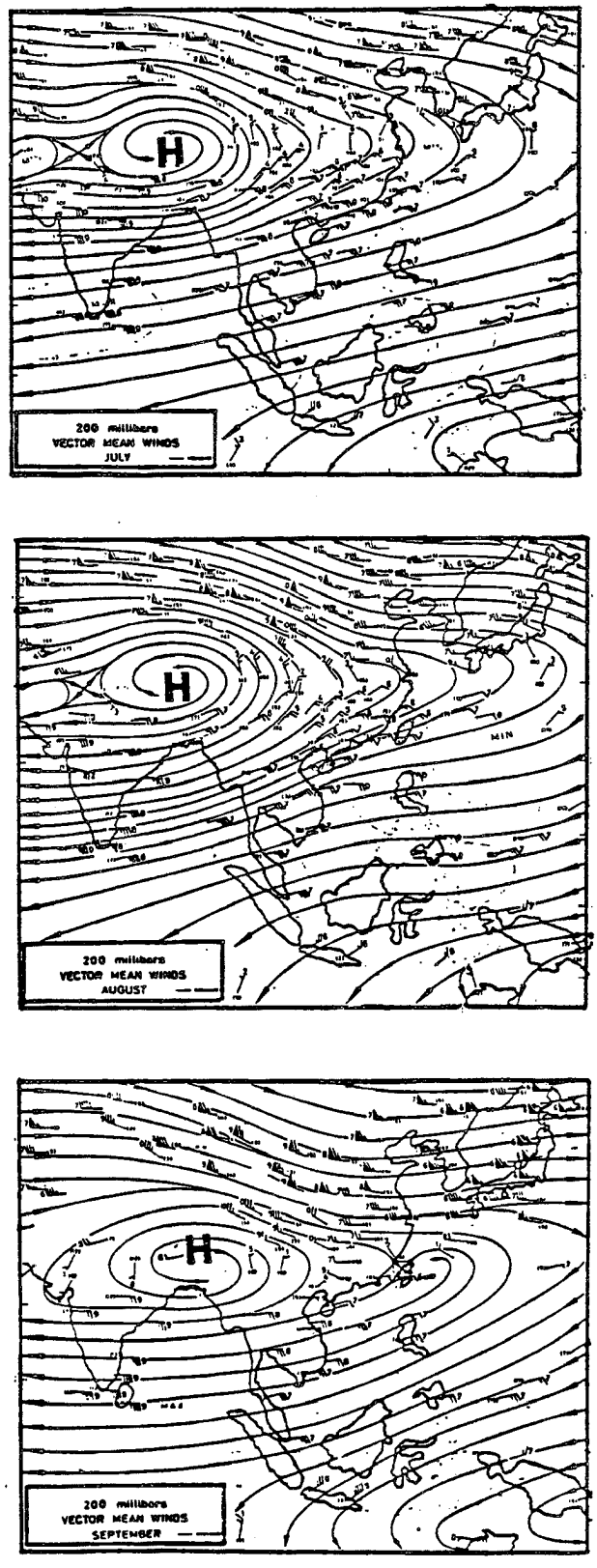

Figure 1.2. Movement of the Tibetan High, Krishnamurti and Bhalme, 1976.

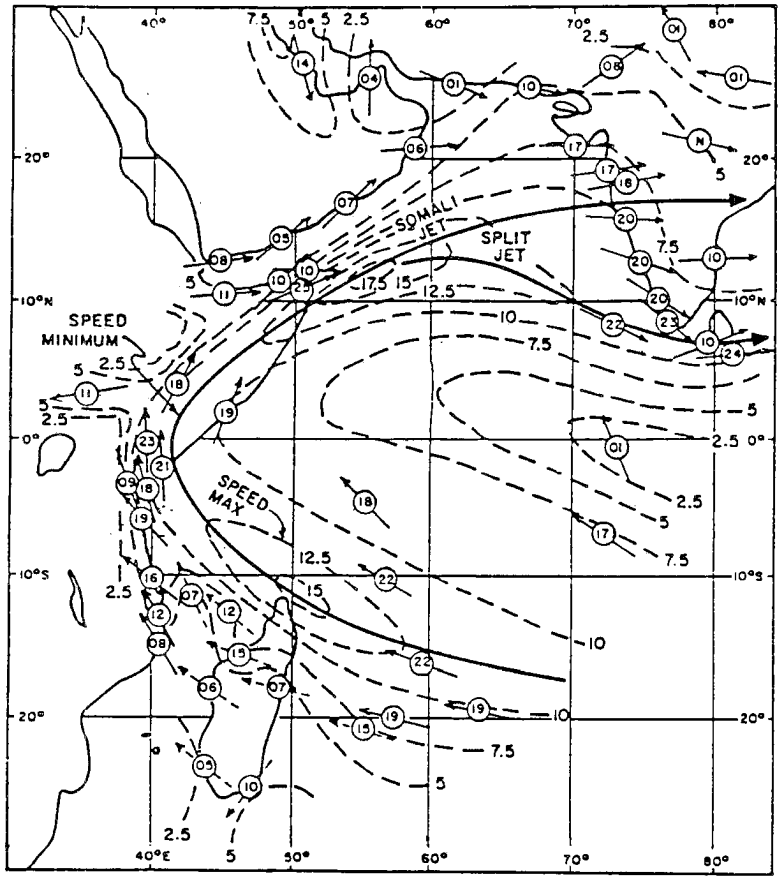

Figure 1.3. The low-level cross equatorial jet in August, Krishnamurti and Bhalme, 1976.

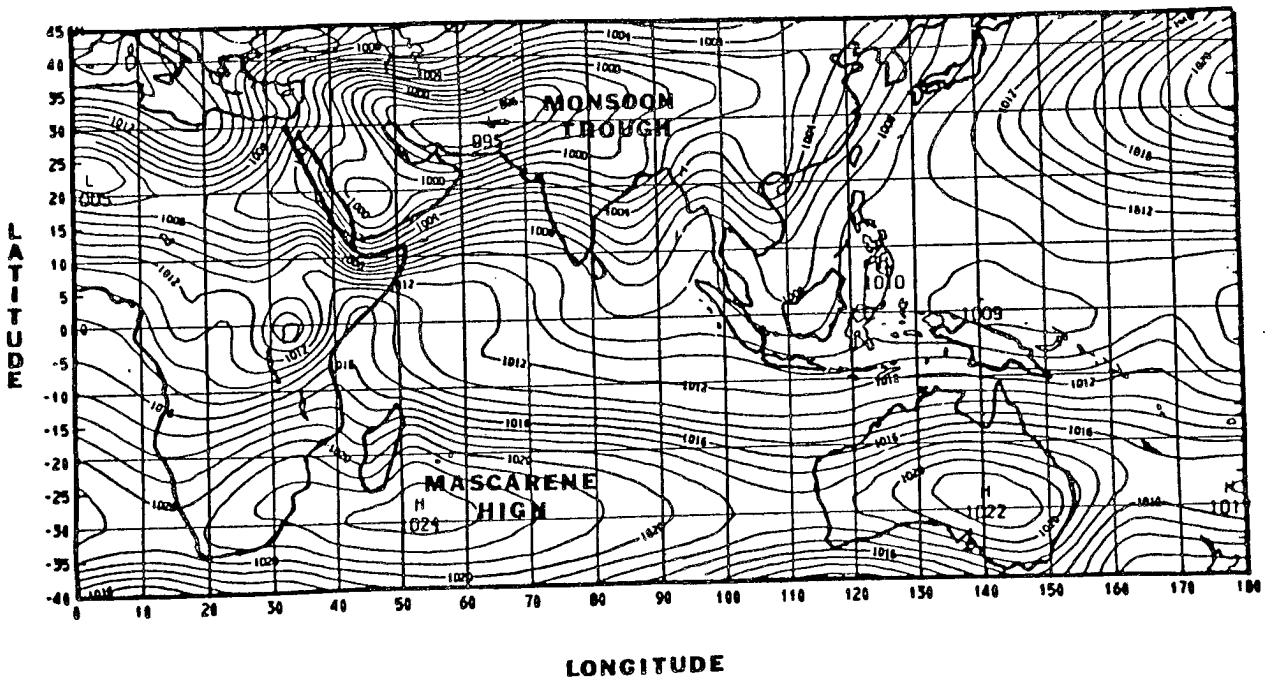

Figure 1.4. Position of the monsoon trough, Krishnamurti and Bhalme, 1976.

low to develop over peninsular India, shifting the anticyclone that had been over the area previously to the Bay of Bengal. Clear skies over the Arabian Sea and the Bay of Bengal also allow for maximum insolation; this insolation when combined with minimal evaporative cooling due to light winds, results in the highest sea surface temperatures in this area for the year (Bunker, 1968). Thus, both the ocean and the land are heating during this period, helping to reduce the land-sea thermal gradient, and thereby slow the change to the summer monsoon circulation. Central and southeast Tibet are almost snow free in the spring, and thus are a heat source for the region, reducing the strength of the subtropical jet flowing to the south, and also reducing the temperature gradient in the north-south direction (Flohn, 1968).

In May, intense heating of the land areas reduces the pressure over Arabia, Pakistan, and north central India, creating heat lows that result in a southwesterly flowing circulation that creates the upwelling off the Somali coast. The resulting drop in sea surface temperature over the western Arabian Sea due to the evaporational cooling acts as an accelerant to the change of the summer monsoon circulation by increasing the thermal gradient between the ocean and land areas (Ramage, pg. 180, 1971).

The summer months (June-September) are marked by the predominance in the large-scale circulation of the southwesterly winds everywhere south of 20°-25° N and the monsoon trough in the overall circulation pattern. The only change in this occurs when, once or twice a season, the monsoon "breaks", and the rains move north to the Himalayan foothills. The onset of the monsoon rains is preceeded by a

substantial weakening of the subtropical jet south of the Himalayas, which, near the time of the onset, makes an abrupt change in location to north of the Plateau. This is apparently caused by the continued action of the Tibetan Plateau as a heat source, and the additional heating caused by condensation in the many thunderstorms in SE Tibet at this time. With the removal of the subtropical jet, this area can be utilized by large scale vertical motions, such as the monsoon depressions that then develop over the Bay of Bengal.

During the summer months the low-level cross equatorial jet is most intense after the onset and frequently splits into two branches, a state which is thought to be caused by barotropic instability in the jet (Krishnamurti and Bhalme, 1976). The jet also acts as the major moisture source for the monsoon, bringing one third of the required moisture from south of the equator, and picking the rest up through evaporation as it moves over the Arabian Sea (Pisharoty, 1965).

In September the intensity of the monsoon circulation steadily decreases, until by October the area is in its transition to the winter monsoon pattern. This transition is characterized by the reappearance and southward movement of the subtropical jet stream, which, when established, runs along the Himalayas to the Yangtze River Valley in China. The Tibetan Plateau re-emerges as a barrier that separates the cold air and wave activity to the north from the sunny, warm Indian Peninsula to the south. In November, the heat low that had been over Pakistan and northern India has been replaced by a weak anticyclone, and the re-establishment of the near-equatorial trough close to 10°N heralds the establishment of the winter monsoon.

To increase the knowledge of the monsoon and its causes one of the sections of the First GARP (Global Atmospheric Research Program) Global Experiment (FGGE), known as the Monsoon Experiment (MONEX), was launched in 1979. This experiment consisted of two parts, winter and summer, and was designed to study the monsoon and the six month pre-monsoonal period (GARP, 1976). The monsoon that year produced subnormal precipitation amounts over the Indian subcontinent, but the major elements of the monsoon circulation were well defined (Fein and Kuettner, 1980).

A major goal of the MONEX project was the definition of heat sources of the monsoon, and long-term heat variations over the monsoon area. From radiation measurements collected utilizing aircraft and satellite platforms the parameters of a radiation budget could be derived. This study will examine the radiation budget at the top of the atmosphere over six months for the period from January to August 1979, using GOES-1 and Nimbus-7 satellite data. The GOES-1 satellite data will be used in equations derived by W. L. Smith, et al. 1981, from a comparison of aircraft and satellite observations. The results given by these equations will then be compared with previously published work on the radiation budget over the southwest monsoon region.

II. DATA COLLECTION AND ANALYSIS

II.A. Data collection

The data used in this study were gathered during the 1979 Monsoon Experiment. There were two parts to this experiment, winter and summer, and it was designed to give a detailed look at the monsoon in its preliminary and mature stages. Observation platforms included aircraft, ships, satellites and ground stations. Radiation measurements were made by aircraft and satellite (GARP, 1976).

II.A.1. The Satellites

For the purposes of the MONEX experiment, a GOES (Geostationary Orbital Earth Satellite) satellite was stationed at 55°E longitude. Data from the satellite were transmitted to a ground station in Villa Franca, Spain; the GOES-1 satellite is operated by the National Environmental Satellite Services (NESS), which also supervised the collection and archival of the data in association with the University of Wisconsin Space Science and Engineering Center (SSEC).

The GOES satellite radiation instrument is a Visible Infrared Spin Scan Radiometer (VISSR), with sensors in the .54 - .7 micron (μm) (visible) and 10.5 - 12.5 μm (IR) wavelengths (Ensor, 1978). The optical system is patterned after the Ritchey-Cretien telescope, 41 cm (16 in.) with polished beryllium mirrors. Once per satellite rotation, the angle of the folding mirror is stepped, a function which is performed by an optical encoder servomechanism. This mirror is used to

deflect the view of the earth approximately 90°. The stepping is .192 milliradian (mr), which gives a resolution of 7 kilometers (km) or 4 nautical miles (n.mi.) near the subsatellite point.

The two kinds of sensors in the VISSR provide visible and IR data at regular intervals. Eight photomultiplier tubes are employed for sensing in the visible with two mercury-cadmium-telluride detectors (Hg-Cd-Te) to sense in the infrared. Since this study utilizes the visible data only, we will look at that part of the satellite in detail.

The area viewed by the .192 mr step is scanned by the eight parallel visible detector channels. Visible brightness signals are then transmitted to the eight photomultiplier tubes by eight fiber optic bundles positioned in the telescope focal plane. The tubes then transform the video information to electrical signals and amplify it. After 1821 scan lines, a "full disk" picture is completed. At the usual scan rate of .6 seconds per scan, a new picture is completed approximately every twenty minutes. This instrument has an instantaneous geometric field of view of .025 x .021 mr.

The other satellite utilized for this study was the Nimbus-7 satellite with the Earth Radiation Budget (ERB) package. Nimbus-7 is a sun synchronous polar orbiting satellite, with passes in the ascending mode at 12 noon LST, and descending mode at midnight. The ERB consists of several different types of instruments which, when combined, give the user the capability to derive the radiation budget for both small and large areas (Madrid, 1978). This study used the narrow angle IR channels 19-22, which measure the earth emitted energy in the 5μm to >50μm bandpass. The scan head is cylindrical and contains four

telescopes that are aligned so that their center lines are 12° apart when projected on a horizontal plane. This scan head has a step of .25°, with each of the telescopes having a rectangular IFOV of .25 by 5.12 degrees, the narrow angle side being in the direction of vertical motion. The detector is a defocussed pyroelectric element immune to solar exposure. (The element is defocussed to obtain uniformity in the field response.)

II.A.2.The Aircraft - (Convair-990)

Aircraft measurements were an important part of the MONEX radiation experiments. These measurements were taken on board NASA's Convair-990 high altitude jet. The aircraft was equipped with three different types of radiometric instruments. There were four Eppley precision spectral pyranometers mounted on the fuselage of the aircraft, along with two pyrgeometers and two instruments for the measurement of angular radiances (Ackerman & Cox, 1980).

The pyranometers measured solar radiation in two spectral ranges; the .3 - .7 μm pyranometers were to be in approximately the same spectral bandpass as GOES-1, and the .3 - 2.8μm pyranometers were to be used to convert visible spectrum data to "total solar" spectrum data. These bandpasses were chosen to calibrate the GOES-1 data, and to convert it to broadband, angularly integrated, reflected solar radiation fluxes. One of each type was mounted on both top and bottom of the fuselage to monitor incoming and upwelling fluxes, respectively.

II.B. Data Analysis

As mentioned previously, the satellite data are archived at the University of Wisconsin, SSEC. These data were initially stored on video cassette magnetic tapes. To put the tapes into a format that

could be used in this study, two major changes had to be performed. The first was the adjustment from a full disk image to a section of that image centered over the MONEX area, approximately 30°N to 30°S, and 25°E to 110°E. The other change was a recording of the regional image onto reel to reel magnetic tapes. The reel to reel tapes, in turn, were used to create visual images on the Colorado State University Department of Atmospheric Science's COMTAL vision one/20 imaging system. Images were taken for seven days each month (consecutive, if possible) at the same time (in GMT) and the pixel value averages were then used in Smith's equations to be converted to albedos and averaged. (Actual days used can be seen in Appendix A).

II.B.1. The Albedo Equations and Their Application

Preparing the image for data analyses, and the analyses themselves took several steps. A procedure was developed to take the GOES-1 brightness data and transform it into useful radiation parameters. The set of equations used to derive albedo from the GOES-1 satellite were first published, as a part of a set of equations to take narrow band (GOES-1) measurements and transform them to integrated broadband values, by W. L. Smith, et al., of the University of Wisconsin, Madison, 1981. These equations were derived from a comparison of the satellite data with aircraft data. Smith (1981), overlaid the CV-990 aircraft's flight plans on GOES-1 images and matched the reflectance values. This was done for five flights over varying terrain: ocean, desert, vegetated land, and clouds. The flight track was superimposed on images ten minutes apart for the best space and time comparisons. The comparison was done manually to insure that conditions were homogeneous within the fields of view of both satellite and aircraft

radiometers. Table 2.1 lists the series of equations used by Smith to derive the albedo. Only equation 1 depends directly on GOES-1 data. The other equations were derived from the multispectral radiometer (MSR) 0.3 - 4.0 μm and 0.5 - 0.9 μm directional radiances measured on the CV-990 aircraft (2), and simultaneous small view angle 0.3 - 4.0 μm MSR and 0.3 - 4.0 μm flux pyranometer observations.

In this study Smith's equations were applied to GOES-1 data. Since the equations require stratification by scene type (ocean, desert, vegetation, and clouds), the MONEX region was partitioned into 23 areas with these limitations in mind. The Köppen and the Thornthwaite systems of climate classification were used (Trewartha & Horn,1980; Griffith, 1972). The Thornthwaite system is especially good for this type of stratification since it is based on the vegetation of a region. The 23 areas are shown in figure 2.1. There are three desert areas (DAF, ME, SA), four vegetated areas (CIN, EIN, WIN, VAF), and sixteen ocean areas. The central latitude and longitude of the areas was ascertained for the computation of the solar zenith angle, an important variable in equation 1. The need to minimize variation of the zenith angle led to partitioning of the ocean region into so many areas. The data sets were arranged so that each area was identified with its Julian Day and its corresponding GOES-1 brightness count. Then the brightness count was converted to the albedo and the albedo was averaged over the area for the seven days used each month (five in February).

To separate the clouds from the other surfaces, threshold values were set. This was done by visually noting low brightness clouds' values and checking them against the highest brightness land or ocean pixel

Table 2.1

Results of Regression Analysis Used to Determine GOES-1 Albedo and Longwave Flux Calibration Relations

	Equation	Surface
1:	$r_g = 0.0000164\ C_g - 0.00077$	All
2:	(a) $r_b = 0.749\ r_g + 0.01747$	Ocean
	(b) $r_b = 0.600\ r_g + 0.08849$	Thick Cloud
	(c) $r_b = 0.840\ r_g + 0.03116$	Vegetation
	(d) $r_b = 0.781\ r_g + 0.08399$	Desert
3:	$A = 1.174\ r_b$	All

where

C_g = the square* of the digital brightness (0-255) obtained from the GOES-1 visible channel detectors divided by the cosine of the solar zenith angle and the earth-sun distance factor.

r_g = Reflectance for the GOES-1 spectral region (0.5-0.9 μm) as measured from CV-990.

r_b = broadband (0.3-4.0 μm) reflectance as measured from CV-990.

A = broadband angularly integrated albedo as measured from CV-990.

*The digital brightness count is generated from a function of the square root of the detector output (radiance).

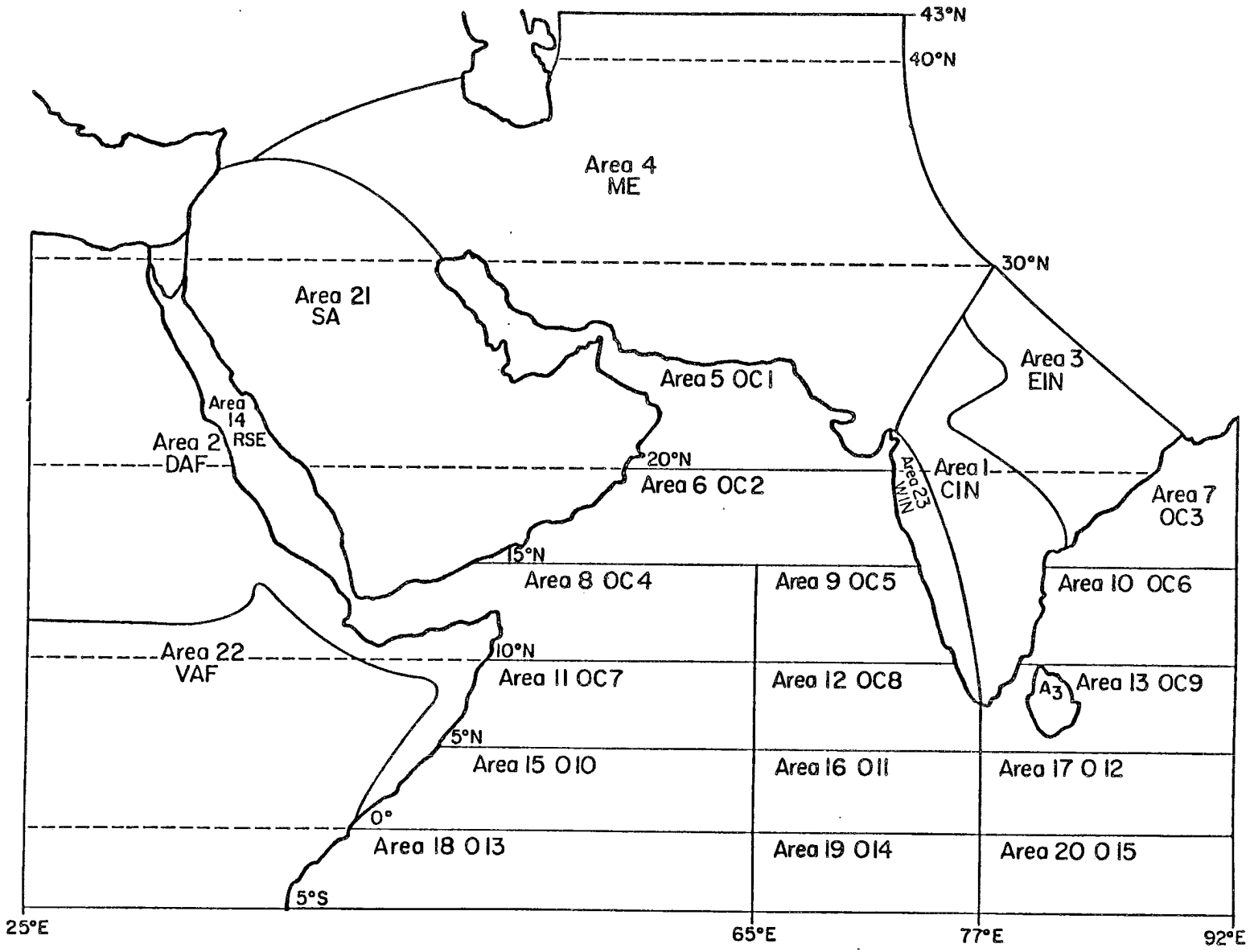

Figure 2.1 - Albedo Areas

value (chosen visually, with a numerical check) in an area. These values could then be reaffirmed by inspecting a histogram representation of the brightness data. This same procedure was used to separate water from land. The threshold values for the different types of areas are given in Table 2.2. Clouds were considered to be any brightness count value greater than the upper threshold value.

Table 2.2.

	Low Pixel Value	High Pixel Value
Desert	60	130
Ocean	20	80
Vegetation	45	100

For the first day of every data set, the limits were checked to see if they were still valid. Since data were taken in the 11-11:30 GMT time period, the extreme eastern section, comprising India and half the Middle East, received very little insolation in January and was consequently darker than the other months. Therefore, the thresholds had to be decreased to assure the correct value for the brightness count average. It turned out that using the ocean threshold values for the India areas and the vegetation threshold values for the Middle East worked quite well. To apply these thresholds, one would isolate one of the 23 small areas on the Comtal screen and then run a program which would give a printed evaluation of the mean, the standard deviation, and a histogram of the pixel values (within the boundaries shown in table 2.2).

Over the oceans a special problem was encountered. The specular reflection of the sun, sunglint, gave certain areas (depending on the sun-satellite geometry) a much higher brightness count, and therefore

albedo, than would normally be expected over water (Davis, 1980)(also see section III.C.). Unfortunately, the sunglint values overlap somewhat with values for thin clouds over water. To determine whether the sunglint is an important influence on albedo, values for albedos, were computed over ocean areas for different zenith angles including and ignoring sunglint effects (data supplied by John Davis). The difference in calculated reflectance between an area when sunglint was included and when it was ignored over zenith angles in the range of 40° to 50° was around 17%. For smaller zenith angles the difference was even greater, with values of 19% for zenith angles of 30° to 40°, and 20% for zenith angles of 10° to 20°. Inspection of actual ocean data revealed the albedo differences between areas when sunglint was included and when it was ignored were as high as 5% (.12 vs. .07). Based upon this evidence the decision was made to keep sunglint in the albedos despite the slight contamination by thin clouds.

III. RESULTS

III.A. Albedo Results

The albedos derived from the GOES-1 data are an interesting part of the overall set of radiation parameters. This is especially true since we have separated the "cloud-free" albedos from the "total" albedos. Monthly values for the cloud-free and actual albedo are presented in figures 3.1-3.6 and table 3.1. One of the more obvious results is the pronounced minimum in both types of albedo in the month of May over most of the study area. An influence on this result might be the fact that there was a cloud minimum over the study region for this period. Among the exceptions for the two types of albedo, the Red Sea area (#15) shows a minimum in February and the Middle East area (#4) a minimum in June. For the albedos with cloud included several of the ocean areas, OC8, O11, O12, and O14, (areas #12, #16, #17, and #19, respectively) have their minima in January due to persistant cloud systems present in the May albedos. This May minimum preceeds a rise in albedo in the June data set, a rise that is quite dramatic on the western coast of India, and the bordering ocean areas. This increase in the complete top of atmosphere (TOA) albedo for the area between 0° E and 115° E and 5° N to 30° N in the first half of June has been previously noted by Winston (1971). In the same study, Winston also noted a pronounced minimum near 35° N by July that persisted through the fall. In 1979, the minimum for the only area that far north (ME, #4) comes in June, and doesn't change much for the remainder

Table 3.1
Cloud Free and Total Albedos

Area	January CF	January T	February CF	February T	May CF	May T	June CF	June T	July CF	July T	August CF	August T
1 CIN	.23	.27	.25	.29	.18	.19	.21	.27	.24	.41	.25	.32
2 DAF	.31	.32	.31	.32	.26	.26	.28	.29	.28	.29	.29	.30
3 EIN	.28	.32	.28	.33	.19	.21	.20	.27	.24	.42	.26	.34
4 ME	.31	.34	.36	.39	.26	.28	.25	.26	.27	.28	.28	.29
5 OC1	.09	.11	.09	.10	.07	.07	.07	.10	.11	.18	.09	.13
6 OC2	.09	.12	.08	.09	.06	.07	.10	.37	.11	.19	.09	.17
7 OC3	.15	.17	.14	.15	.12	.13	.12	.19	.14	.25	.17	.25
8 OC4	.08	.12	.07	.08	.06	.07	.10	.19	.09	.11	.07	.08
9 OC5	.10	.12	.08	.09	.06	.07	.12	.50	.12	.20	.11	.17
10 OC6	.15	.16	.15	.16	.10	.10	.16	.25	.14	.23	.17	.20
11 OC7	.08	.14	.08	.12	.06	.09	.09	.17	.07	.09	.08	.09
12 OC8	.08	.10	.10	.17	.07	.12	.11	.43	.10	.16	.10	.15
13 OC9	.13	.15	.13	.16	.10	.11	.16	.21	.14	.20	.15	.16
14 RSE	.08	.13	.07	.08	.09	.10	.09	.12	.09	.12	.08	.10
15 010	.07	.10	.08	.12	.06	.08	.09	.17	.07	.10	.08	.10
16 011	.08	.09	.09	.15	.08	.11	.11	.19	.09	.12	.11	.18
17 012	.12	.14	.13	.19	.12	.17	.15	.19	.16	.26	.16	.21
18 013	.08	.11	.08	.10	.06	.08	.09	.17	.07	.12	.08	.10
19 014	.08	.11	.09	.19	.08	.12	.11	.18	.09	.15	.11	.18
20 015	.13	.18	.14	.23	.11	.12	.14	.18	.19	.33	.18	.27
21 SA	.38	.39	.37	.37	.31	.31	.31	.31	.32	.32	.33	.33
22 VAF	.17	.23	.17	.22	.15	.19	.15	.20	.15	.20	.16	.22
23 WIN	.19	.21	.21	.24	.15	.17	.21	.44	.22	.33	.23	.33

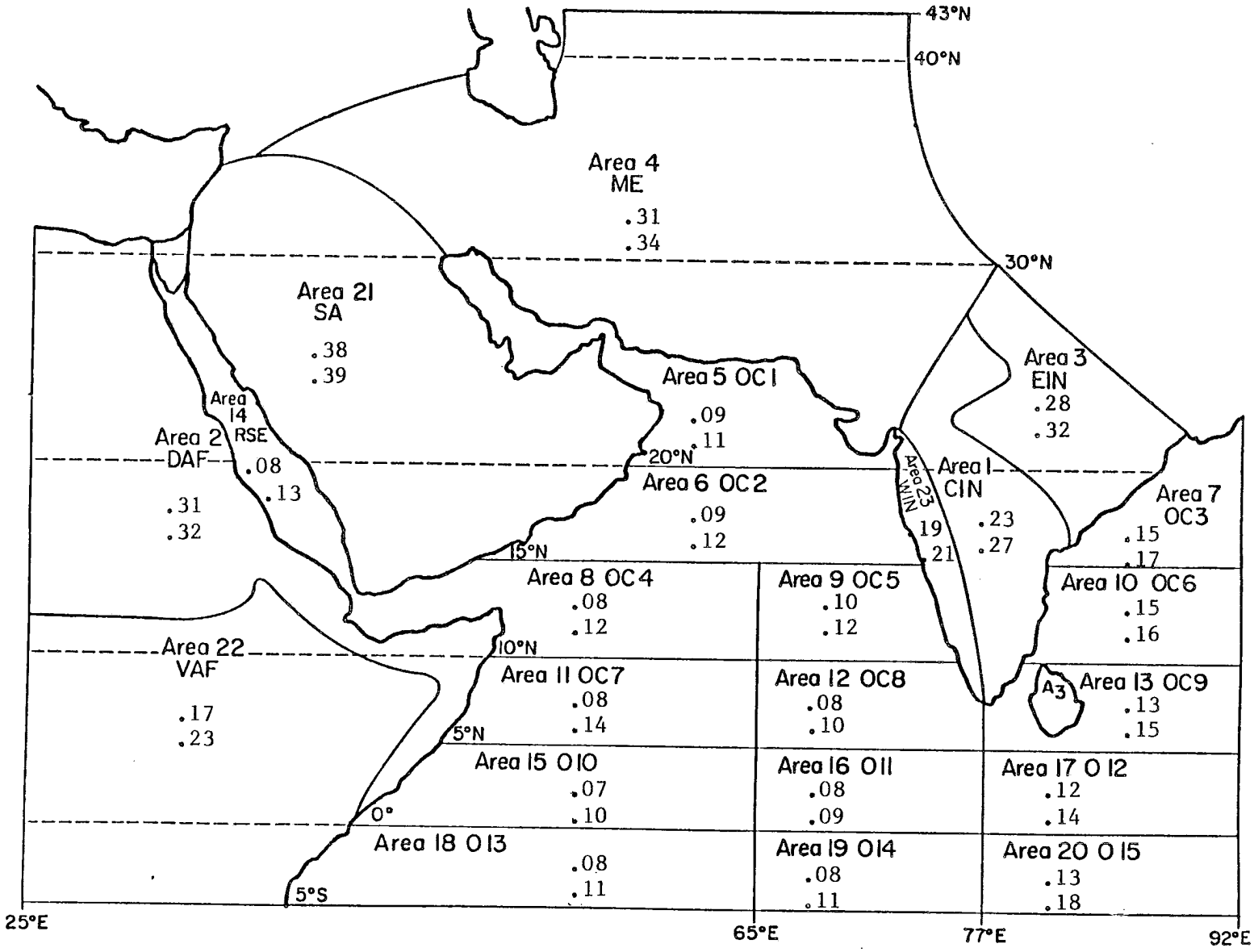

Figure 3.1 - January - Cloud Free Albedos - Total Albedos

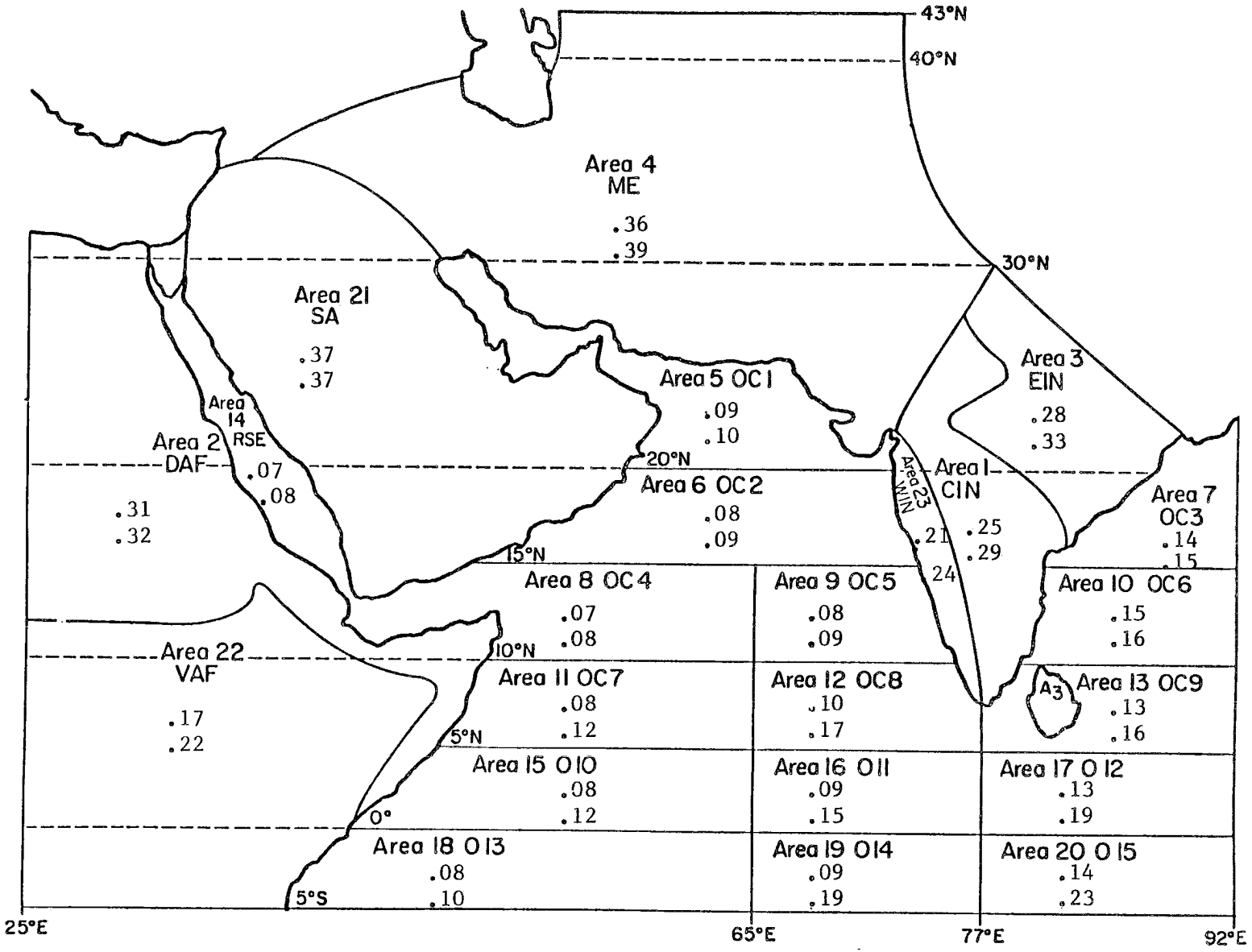

Figure 3.2 - February - Cloud Free Albedos - Total Albedos

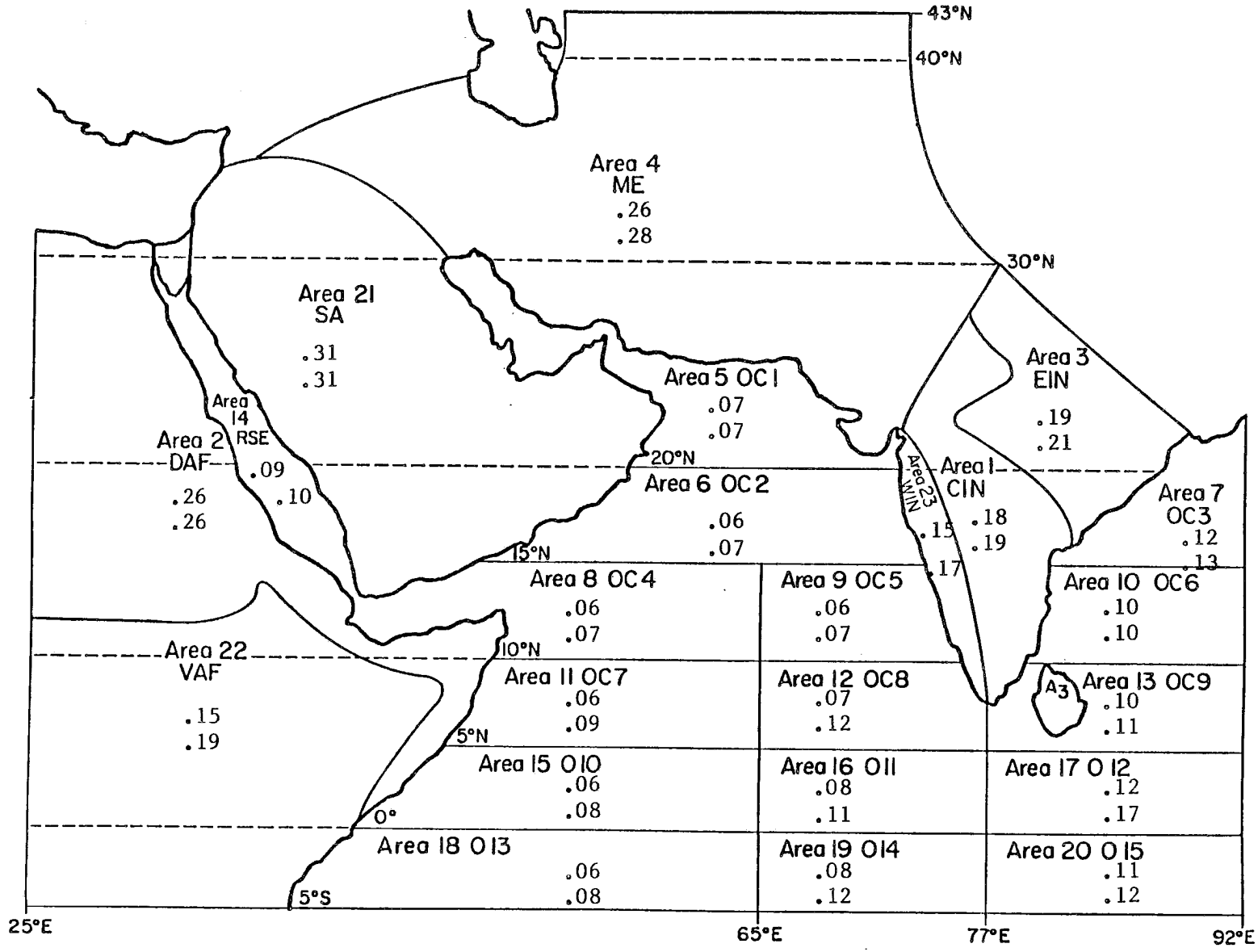

Figure 3.3 - May - Cloud Free Albedos - Total Albedos

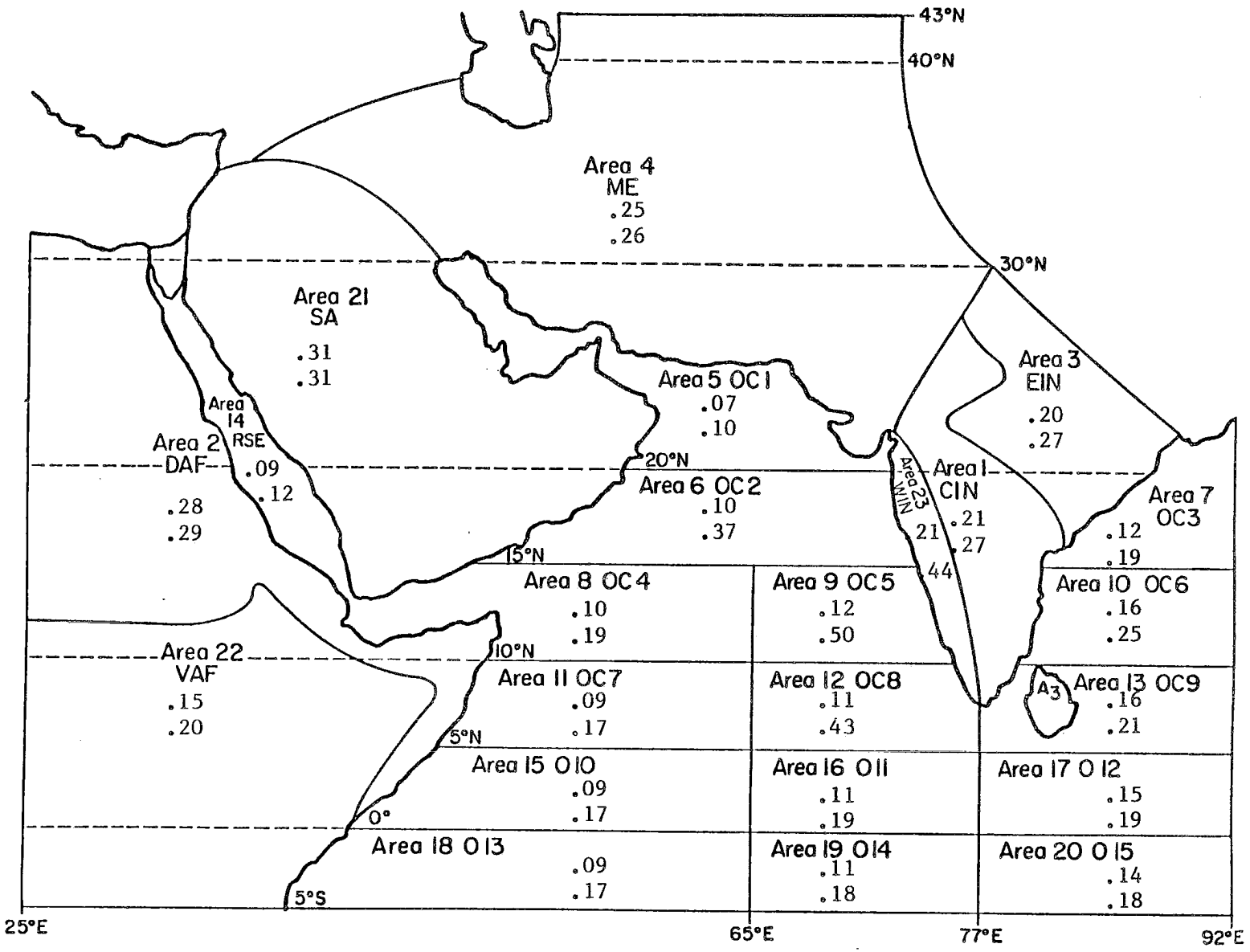

Figure 3.4 - June - Cloud Free Albedos - Total Albedos

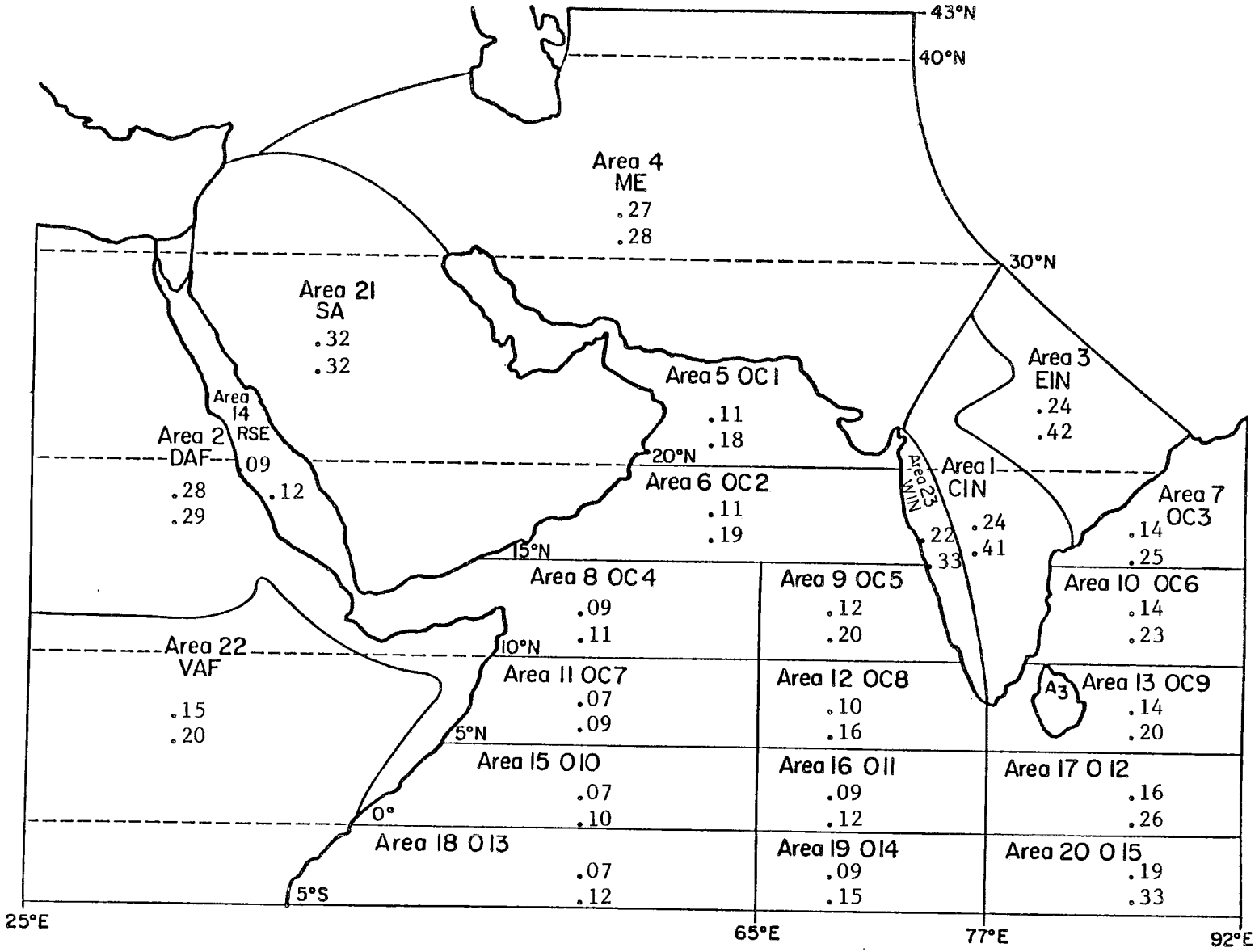

Figure 3.5 - July - Cloud Free Albedos - Total Albedos

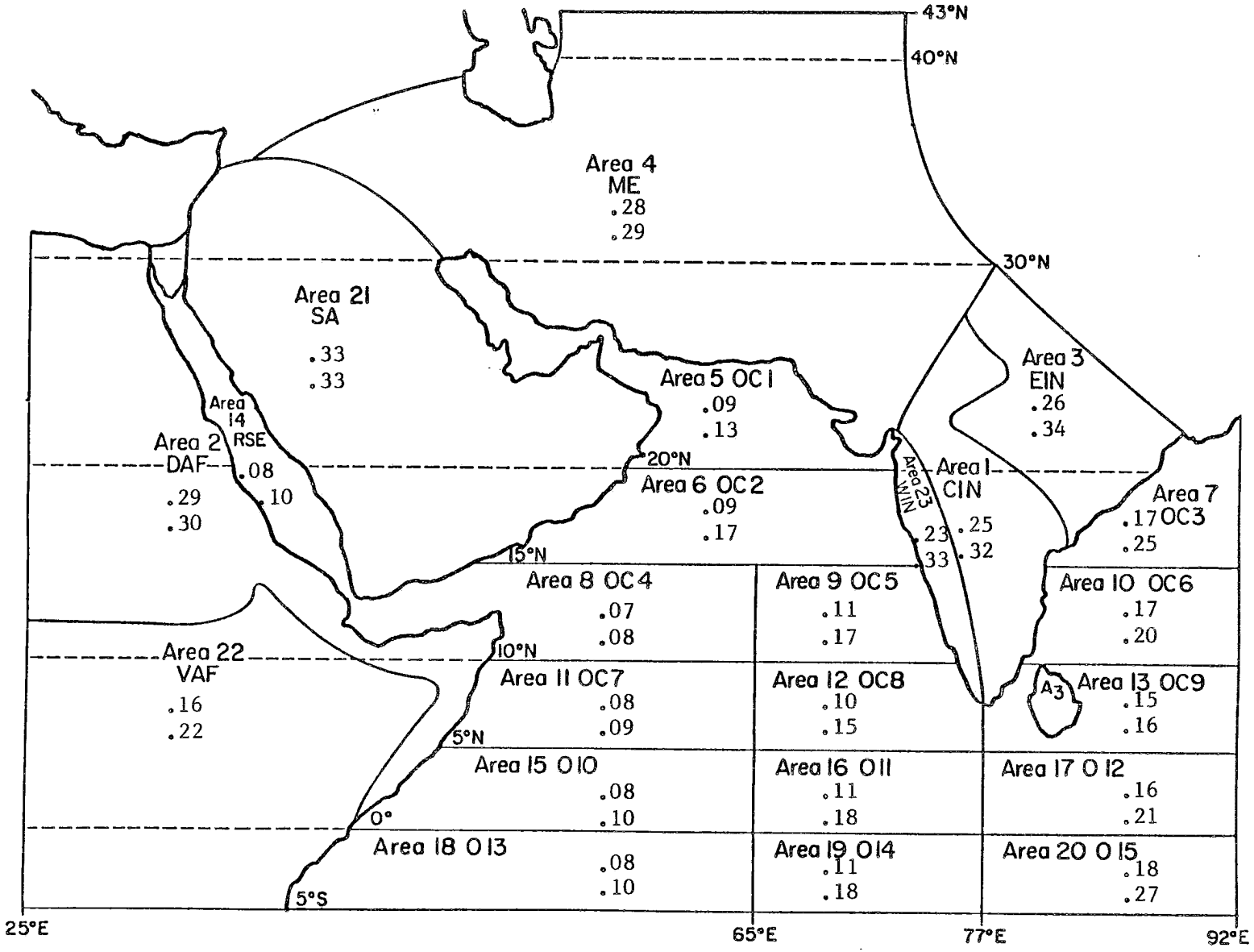

Figure 3.6 - August - Cloud Free Albedos - Total Albedos

of the data set, which is in near agreement with Winston. Winston's data also showed generally lower albedos near the vernal equinox compared with albedos near the spring equinox; this is reflected in the present study by the August albedo values for cloud-free areas being somewhat lower than their February counterparts, however when the clouds are added this relationship seems to break down.

III.B. Radiation Budget Study

The atmosphere can be compared to a giant heat engine (Miller & Thompson, 1975). In the earth-atmosphere system, there are both heat sources and heat sinks resulting in patterns of differential heating. Due to the principle of conservation of heat energy the earth-atmosphere system is constantly trying to bring these areas of differential heating into thermal equilibrium. This results in energy transfer in many different forms, including wind, and therefore the weather. Radiation is the principal source for the heating of the atmosphere (Miller & Thompson, 1975). It is therefore logical that to understand the earth-atmosphere system better, one should be acquainted with the "radiation budget" of the system. Albedos are a major parameter in radiation budgets, along with the incoming insolation and the longwave (LW) radiation emitted from the earth-atmosphere system. The monthly values and changes in the net radiation values in their turn, are valuable parameters in the overall energy budget of the earth-atmosphere system, since deficits must import energy and surpluses must export energy, either through atmospheric processes, or oceanic transport. Using a system of equations taken from Sellers (1965) a program was written to take latitude (ϕ), albedo (α), and LW radiation (w/m^2); and return the shortwave (SW) (w/m^2) and net

radiation (w/m^2). The incident shortwave radiation at the top of the atmosphere (Qs) was calculated using the equation

$$Qs = \frac{1440}{\pi} S(\frac{\bar{d}}{d})^2(H\text{-}\tan H) \sin\phi \sin\delta \qquad (1)$$

where S is the solar constant, d is the earth-sun distance, H equals the half day length, and δ is the declination angle. The net radiation was then calculated with the equation:

$$Net = Qs\ (1-\alpha_T) - LW \qquad (2)$$

The solar constant used in the calculation of the shortwave was 1368 w/m^2, (Smith, E.; personal communication). Monthly averages of LW data for the year 1979 were taken from the Nimbus-7 ERB (Randel, D.; personal communication). The values for the net radiation budget for each of the six months is presented in table 3.2 and in figures 3.7-3.12.

III.B.1. Monthly Summaries

a. January

As would be expected when the sun is to the extreme south of the equator, almost all of the land areas in the study region (which is north of 5° S), with the exception of the equator-straddling VAF(#22), have negative radiative balances in January. Of the ocean areas, only the northernmost two, OC1 (#5) and OC3 (#7) have negative values. Two areas have values quite close to zero, the west coast of India (#23) with -1.67 w/m^2 and the Red Sea with 2.45 w/m^2. The largest surpluses of energy are to be found to the areas south of the equator, which are receiving the most direct insolation.

Table 3.2

Net Radiation (w/m^2)

	Area	January	February	May	June	July	August
1	CIN	-31.85	-28.26	73.28	77.28	37.27	69.2
2	DAF	-52.0	-32.06	22.70	-9.32	-5.87	-5.09
3	EIN	-70.23	-65.83	53.74	67.39	33.15	54.44
4	ME	-67.92	-37.54	47.20	33.73	-1.60	-16.02
5	OC1	-20.36	12.88	118.34	151.46	115.49	132.66
6	OC2	16.99	53.20	117.94	52.57	121.51	116.01
7	OC3	-7.11	29.58	143.68	169.15	137.32	131.64
8	OC4	59.95	78.10	107.66	121.16	111.07	127.11
9	OC5	47.80	80.48	125.61	13.50	106.04	107.22
10	OC6	25.96	63.51	141.90	113.72	129.32	124.52
11	OC7	85.04	98.18	123.07	115.36	109.89	114.27
12	OC8	86.55	79.39	128.05	45.26	122.23	128.01
13	OC9	76.09	96.92	142.86	110.26	114.33	127.0
14	RSE	2.45	37.01	105.13	76.71	81.34	90.68
15	010	119.73	125.21	128.83	106.43	97.29	114.82
16	011	114.13	106.53	138.11	122.78	124.05	121.54
17	012	108.93	118.07	111.01	104.88	76.03	117.35
18	013	146.89	138.52	98.46	72.07	70.91	92.02
19	014	142.03	124.46	99.35	93.03	96.80	117.95
20	015	119.73	136.48	96.95	87.69	33.61	105.66
21	SA	-71.60	-79.30	11.44	-15.05	-28.93	-19.37
22	VAF	61.61	97.26	83.72	66.13	61.71	71.46
23	WIN	-1.67	-2.07	79.08	-.032	68.71	63.71

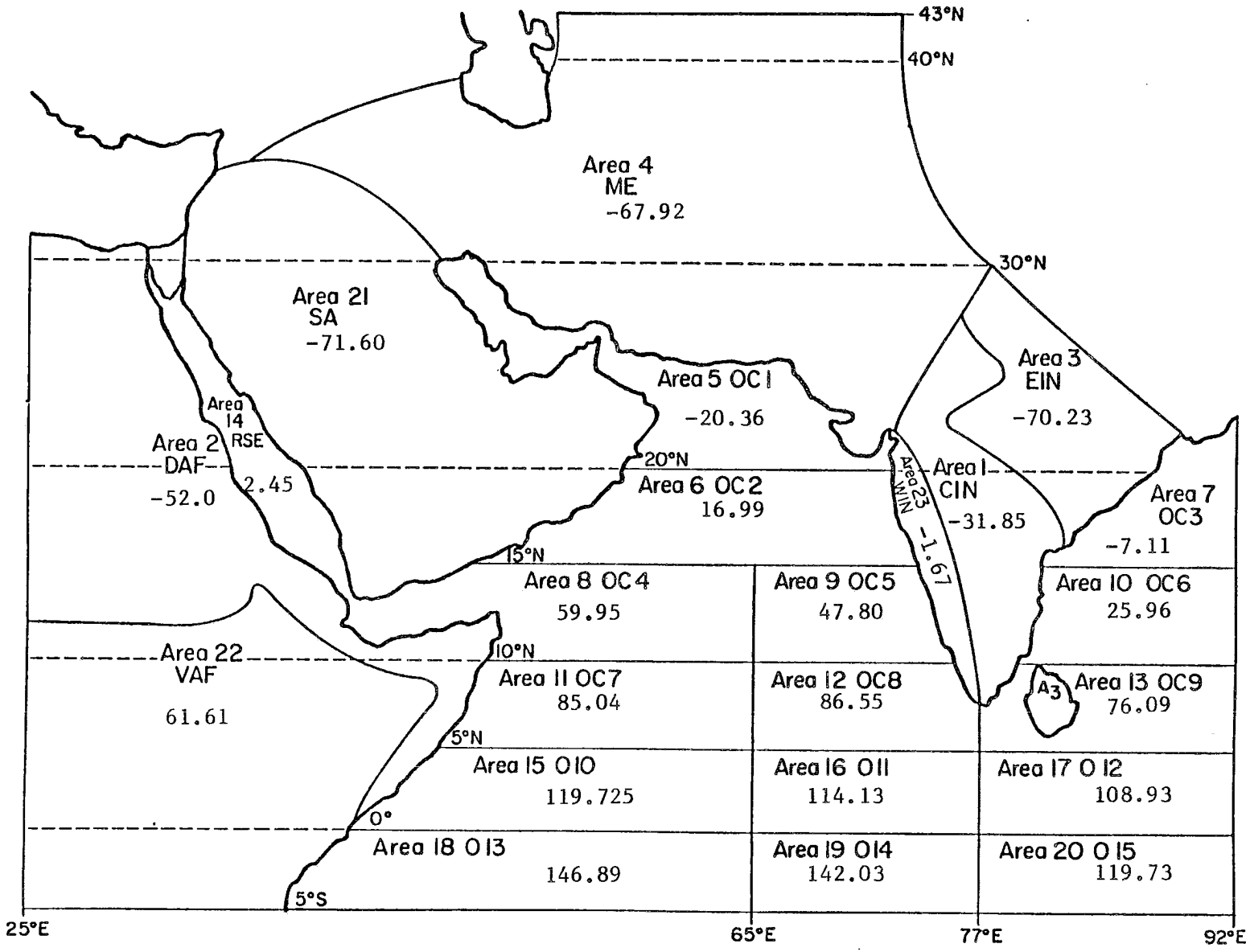

Figure 3.7 - January (015) - Net Radiation (w/m^2) - (daily value)

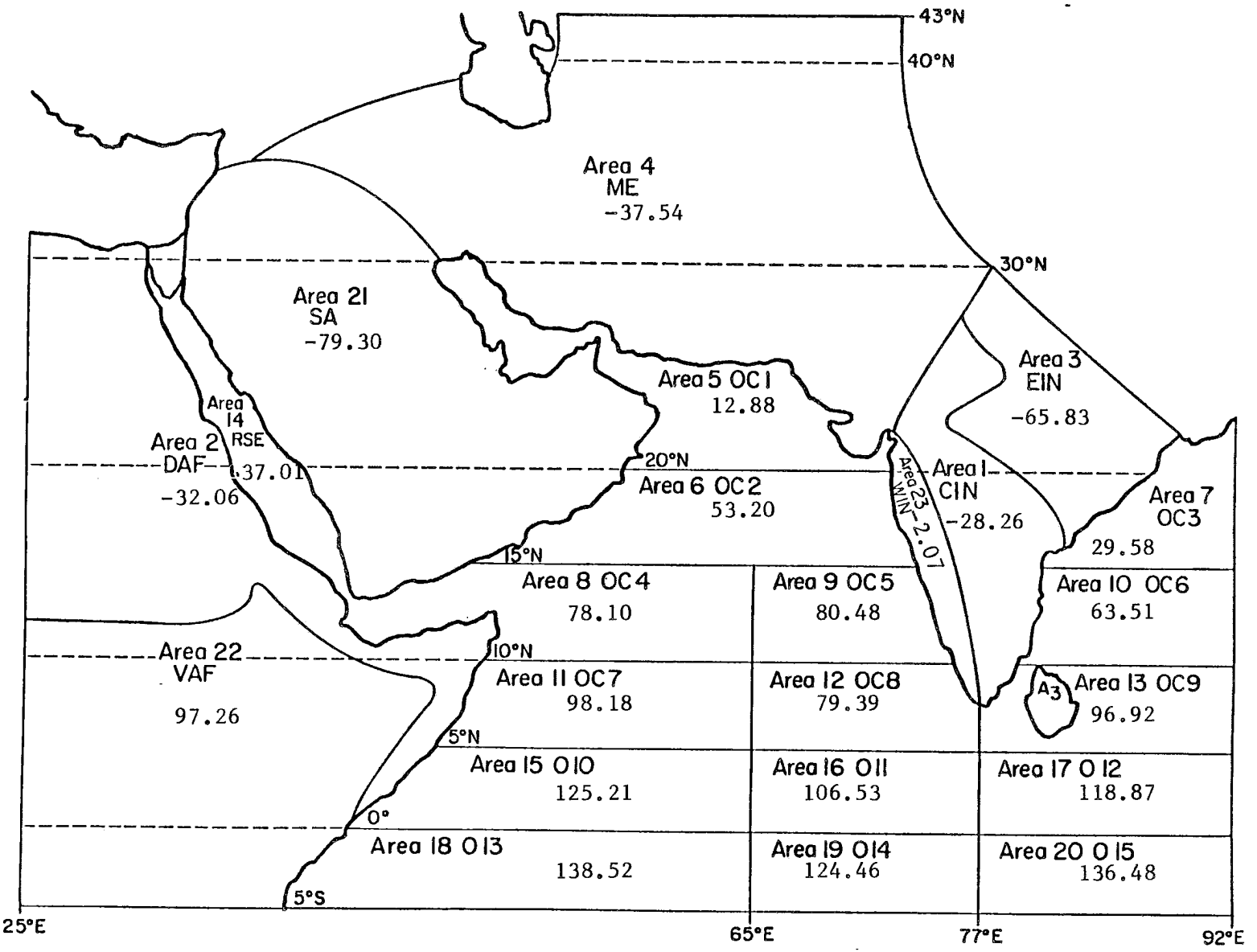

Figure 3.8 - February (046) - Net Radiation (w/m^2) - (daily value)

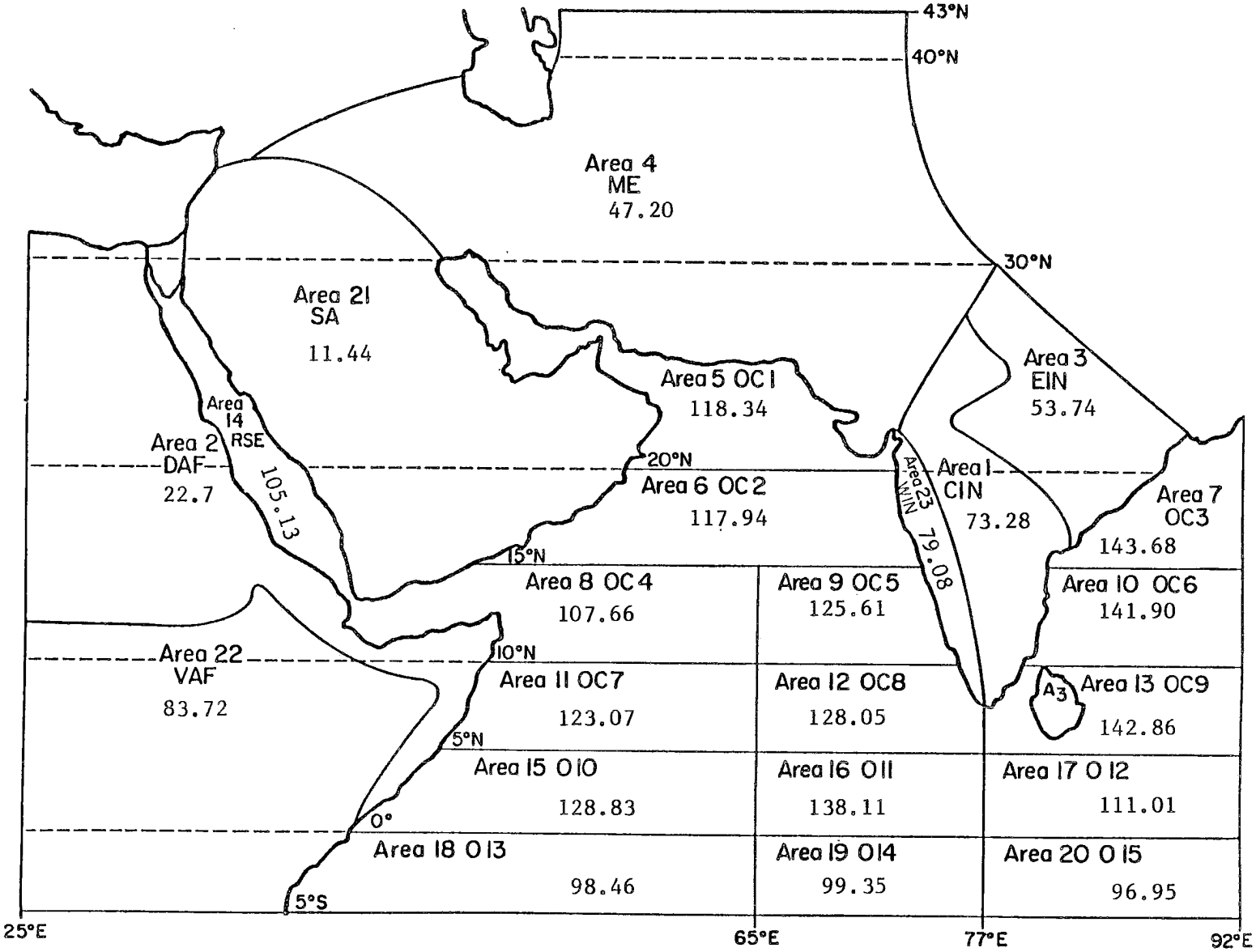

Figure 3.9 - May (135) - Net Radiation (w/m^2) - (daily value)

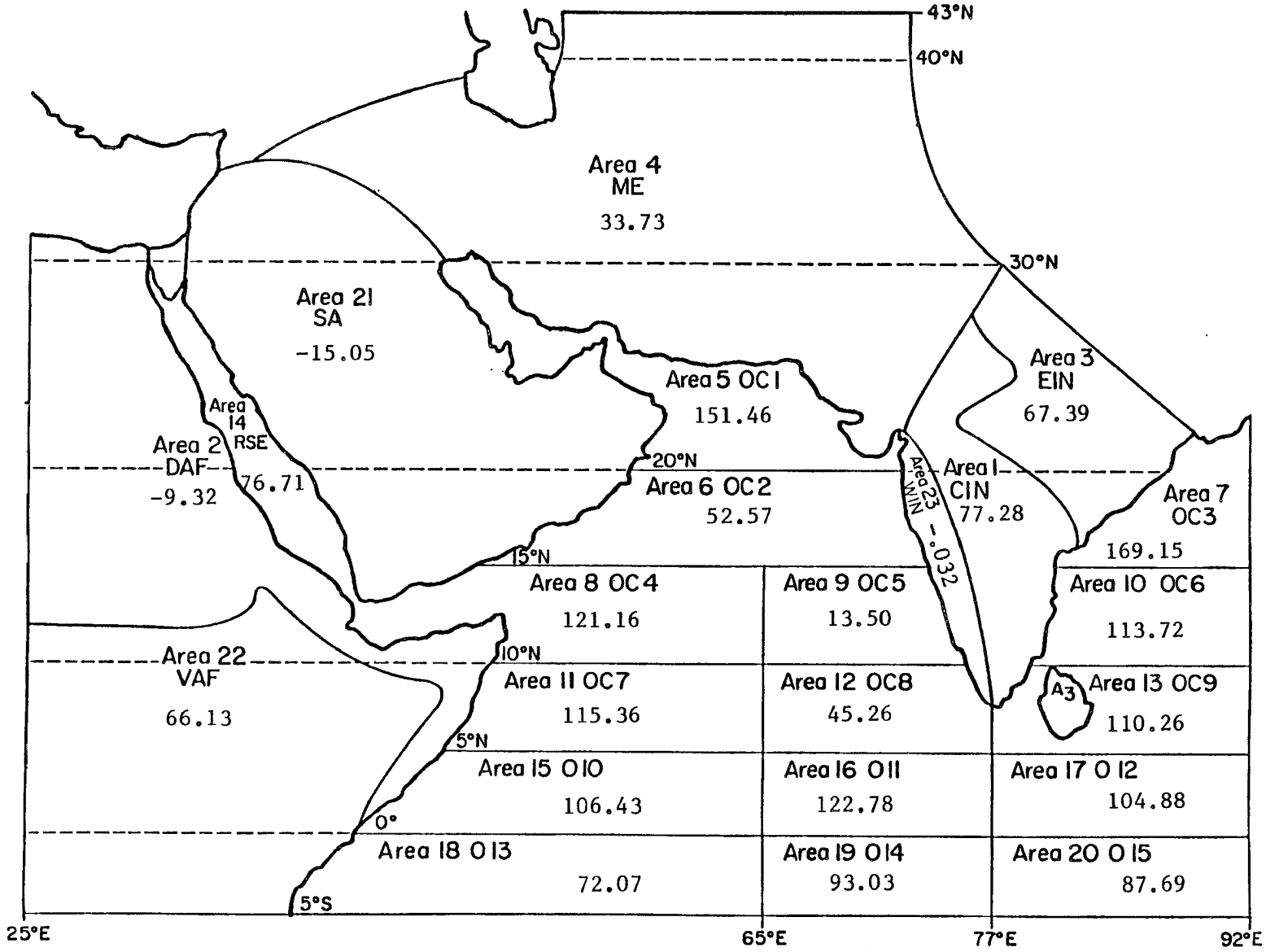

Figure 3.10 - June (166) - Net Radiation (w/m^2) - (daily value)

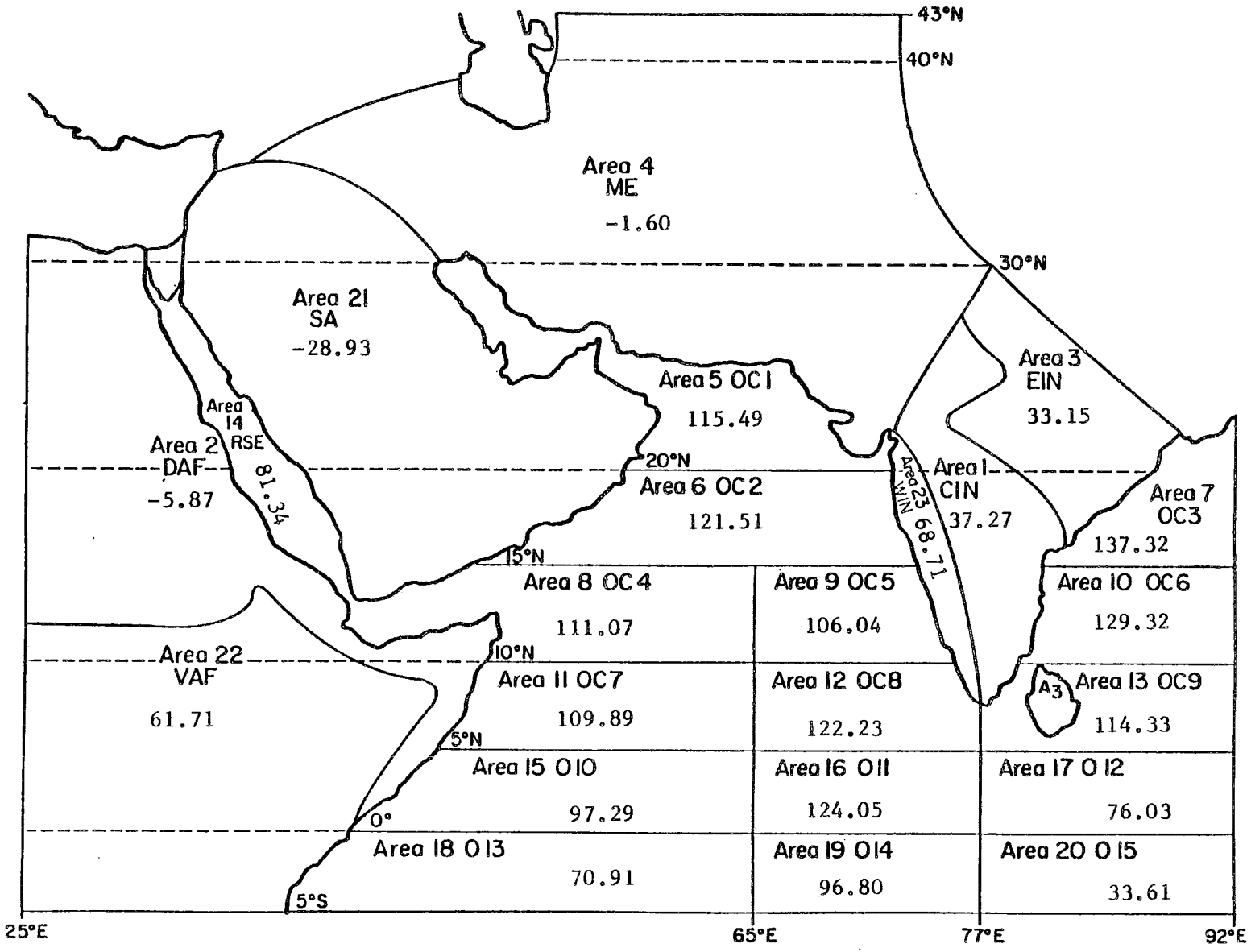

Figure 3.11 - July (196) - Net Radiation (w/m^2) - (daily value)

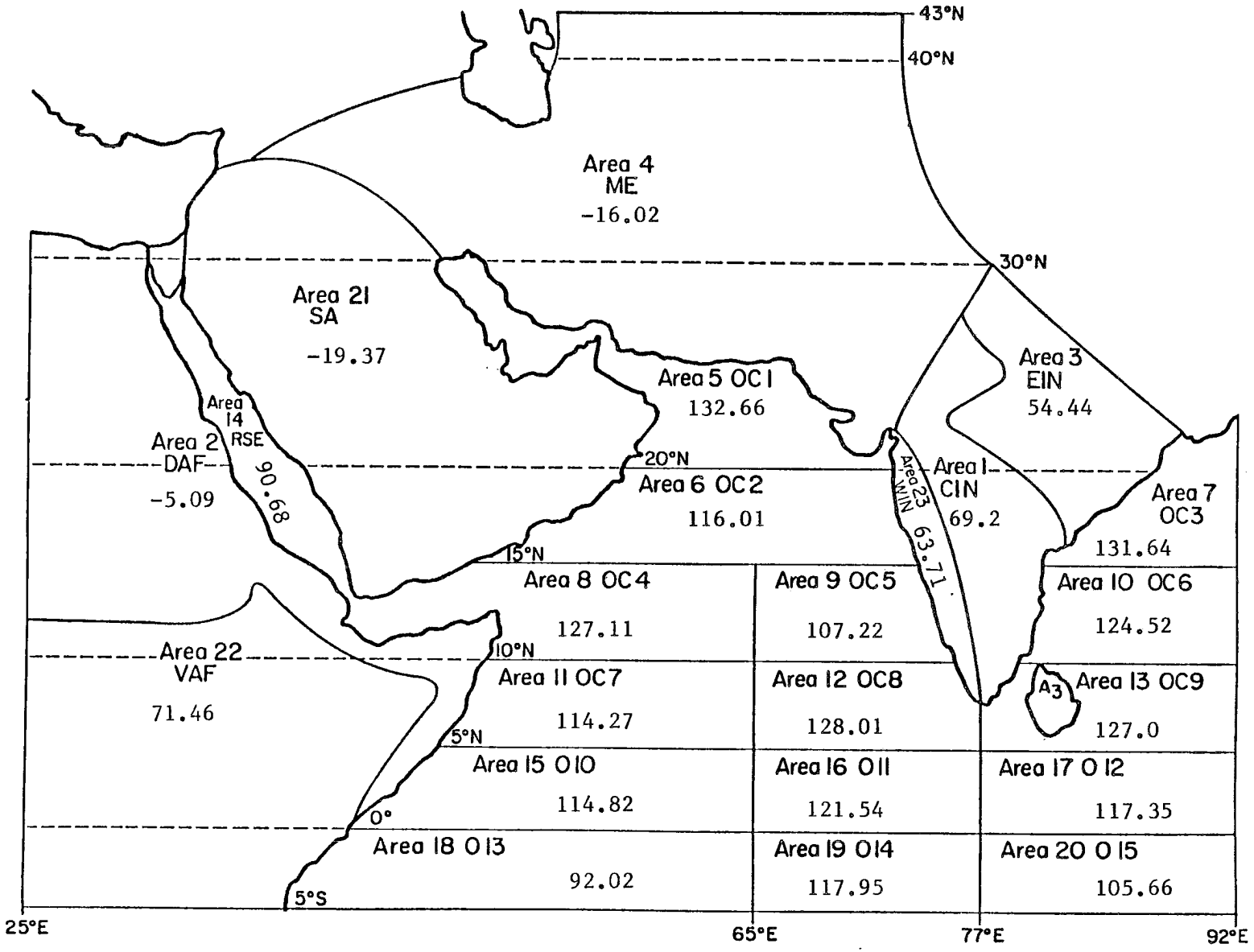

Figure 3.12 - August (227) - Net Radiation (w/m^2) - (daily value)

One way the atmosphere can attempt to compensate for a radiative imbalance is through vertical motion. Subsidence warms the air through compression, and is a response to a radiation deficit. The opposite, rising motion, occurs in areas with surpluses. In the month of January, this response ranges from a large value of subsiding motion over Saudi Arabia of -205.5 meters per day (m/d) for a 900 mb layer, and over the area with the largest surplus, 013 (#18), there is a potential for a great amount of rising motion, with a value of 423.3 m/d.

b. February

With the sun's migration northward, fewer areas are reporting deficits. All of the ocean areas are now in the positive category. However, the same land areas are still recording slightly smaller deficits. The largest surpluses in net radiation are still south of the equator, and the largest deficits are in Saudi Arabia (SA, #21) and east India (EIN, #3). Four areas had a decrease in net radiation from the previous month, OC8 (#12), 011 (#15), SA(#21), and WIN (#23). The changes in the ocean areas were due to an increase in total albedo, and the changes over the land areas were due to increases in the outgoing longwave radiation. In this month, the possible amounts of radiatively forced vertical motion have extremes of -227 m/d in SA (#22), and 398.78 m/d in 013 (#18).

c. May

A dramatic change takes place in the time interval between February and May. By the time of the May sample every area has a surplus of energy, including the deserts. The surpluses over the deserts are quite small, while the largest surpluses appear over the

easternmost ocean areas. Changes from the previous month include major gains in net radiation in areas; CIN (#1), WIN (#23), ME (#4), OC1 (#5), and OC3 (#7). The primary reasons for this change is a decrease in albedo and increase in the shortwave radiation. WIN (#23) and OC3 (#7) also had less longwave radiation outgoing. Due to the decrease in insolation south of the equator, areas O12 (#17), O13 (#18) and VAF (#22) were the only areas to have less of a surplus than the previous time period. As a result of the net radiation having all positive values, the compensating vertical motions in May are only rising motion. SA (#22) again has the minimum, 32.88 m/d, and the area of greatest net radiation was OC3 (#6), with a potential for 414.1 m/d of rising motion.

d. June

The month of the onset of the monsoon has some interesting features. The albedo data was taken from the week of onset, June 15-21. Of particular interest is a very small negative value for the west India coast (WIN, #23). In fact, the area is less than 1 w/m^2 from being in balance. The surrounding ocean areas (OC5, #9; and OC8, #12) have positive values, but they are much less than any of the other ocean areas. The areas with the greatest surpluses are OC1 (#5) and OC3 (#7), probably because they have less cloud cover (lower albedo) than their ocean neighbors. Another effect that seems to be cloud related is the fact that almost every area had less of a surplus than in May except five, CIN (#1), EIN (#3), OC1 (#5), OC3 (#7), and OC4 (#8). In the land areas the gains in surpluses were due to outgoing LW decreases despite slightly higher albedos. Over the ocean areas all except the Red Sea area (#16) had less LW loss, but most of the areas

that have less of a surplus had a healthy gain in albedo from the previous month due almost exclusively to clouds. The vertical motion field for June is also quite interesting. The minimum/maximum radiation values are again over Saudi Arabia and the Bay of Bengal, with resultant possible vertical motions of -43.26 m/d and 484.66 m/d, respectively. The area near, and including the west Indian coast is an area of local minimums, and representative motions over that area are -.092 m/d over WIN (#23), and 37.36 m/d over OC5 (#9). Since typical values for the type of convection found in this area are much greater than these values of rising motion, one can conclude that the major energy source in these areas at this time is condensational.

e. July

The data for July were taken during one of the monsoon breaks, which occurred around July 13 and continued for approximately two weeks; this break was concurrent with the intense convection in the near equatorial trough, which appears in this study as an albedo maximum - net radiation minimum in area 015 (#20), (Fein and Kuettner, 1980). The net radiation values for the desert areas are all negative in this month. North Africa (DAF, #2) is slightly less negative than in June, but the other two areas (SA, #21; ME, #4) have increased their deficits. The India areas, with albedos of 30 to 40 percent, are all positive, but have rather low values. The greatest surpluses are in the ocean areas OC2 (#6), OC3 (#7), OC6 (#10), OC8 (#12), and 011 (#16). These areas (with the exception of OC3 (#7) which had slightly less energy) also were some of the biggest gaining areas for July, along with WIN (#23). With the increase in energy in area WIN, the vertical motion changes sign also, and the compensational vertical

motion becomes 197.49 m/d, quite an increase. SA (#22) increases its possible subsident motion to -83.15 m/d, and OC3 (#7) drops to 395.71 m/d.

f. August

Led by the Middle East region (#4), the deficits in the deserts increase in August. The ocean areas are all very similar, with the range of values clustered between 90 and 132 w/m^2. These areas also have the largest surpluses, with OC1 (#5) and OC3 (#6) having the greatest. O15 (#20) dramatically increases its surplus due to increased insolation and decreased LW out and albedo. India also seems to be reaching a state of equanimity, with the three areas having similar values. Representative values of the potential vertical motion over each type of surface are 380.37 m/d over OC1 (#5), 183.12 m/d over WIN (#23), and -55.2 m/d over SA (#22).

III.B.1a. Areal Net Radiation

If one multiplies the net radiation by the actual area of the region, the result is an areal net radiation value. This value gives one a feeling for the actual amount of energy the region needs to import, if the value is negative, or the amount of surplus energy to be exported if the value is positive. Figures 3.13 - 3.18, and Table 3.3 illustrate the areal net radiation for each area for the six months studied, and also the total for the monsoon region itself for each of those months. An inspection of these values shows that this region is definitely a radiative heat source region. The month of May is the month of greatest total areal value, with 237.736×10^{13} w, and January shows the minimum value for the months studied, with only 43.24×10^{13} w total output. It is interesting to note the sharp decrease

Table 3.3

Areal Net Radiation (w x 10^{13})

	Area	January	February	May	June	July	August
1	CIN	-1.70	-1.51	3.91	4.12	1.99	3.69
2	DAF	-1.58	-9.73	6.89	-2.83	-1.78	-1.55
3	EIN	-10.27	-9.62	7.86	9.85	4.85	7.96
4	ME	-2.90	-16.02	20.14	14.39	-.684	-6.84
5	OC1	-1.91	1.21	11.11	14.22	10.85	12.46
6	OC2	1.81	5.66	12.56	5.60	12.94	12.35
7	OC3	-.44	1.84	8.96	10.55	8.56	8.21
8	OC4	6.59	8.58	11.83	1.33	12.21	13.97
9	OC5	2.87	4.82	7.53	.81	6.35	6.43
10	OC6	1.66	4.07	9.09	7.28	8.28	7.98
11	OC7	7.96	9.19	11.52	10.8	10.29	10.70
12	OC8	6.21	5.70	9.93	3.25	8.77	9.19
13	OC9	5.80	7.39	10.89	8.40	8.71	9.68
14	RSE	.11	1.72	4.89	3.57	3.79	4.22
15	010	14.19	14.84	15.27	12.62	11.53	13.61
16	011	8.46	7.89	10.23	9.10	9.19	9.01
17	012	9.42	10.21	9.60	9.07	6.31	10.14
18	013	21.77	20.53	14.59	10.68	10.51	13.64
19	014	10.01	8.77	7.01	6.56	6.82	8.31
20	015	10.35	11.80	8.38	7.58	2.90	9.13
21	SA	-26.03	-28.84	4.16	-5.47	-10.52	-7.04
22	VAF	21.20	33.47	28.81	22.76	21.24	24.59
23	WIN	-.06	-.068	2.59	-.00	2.25	2.08

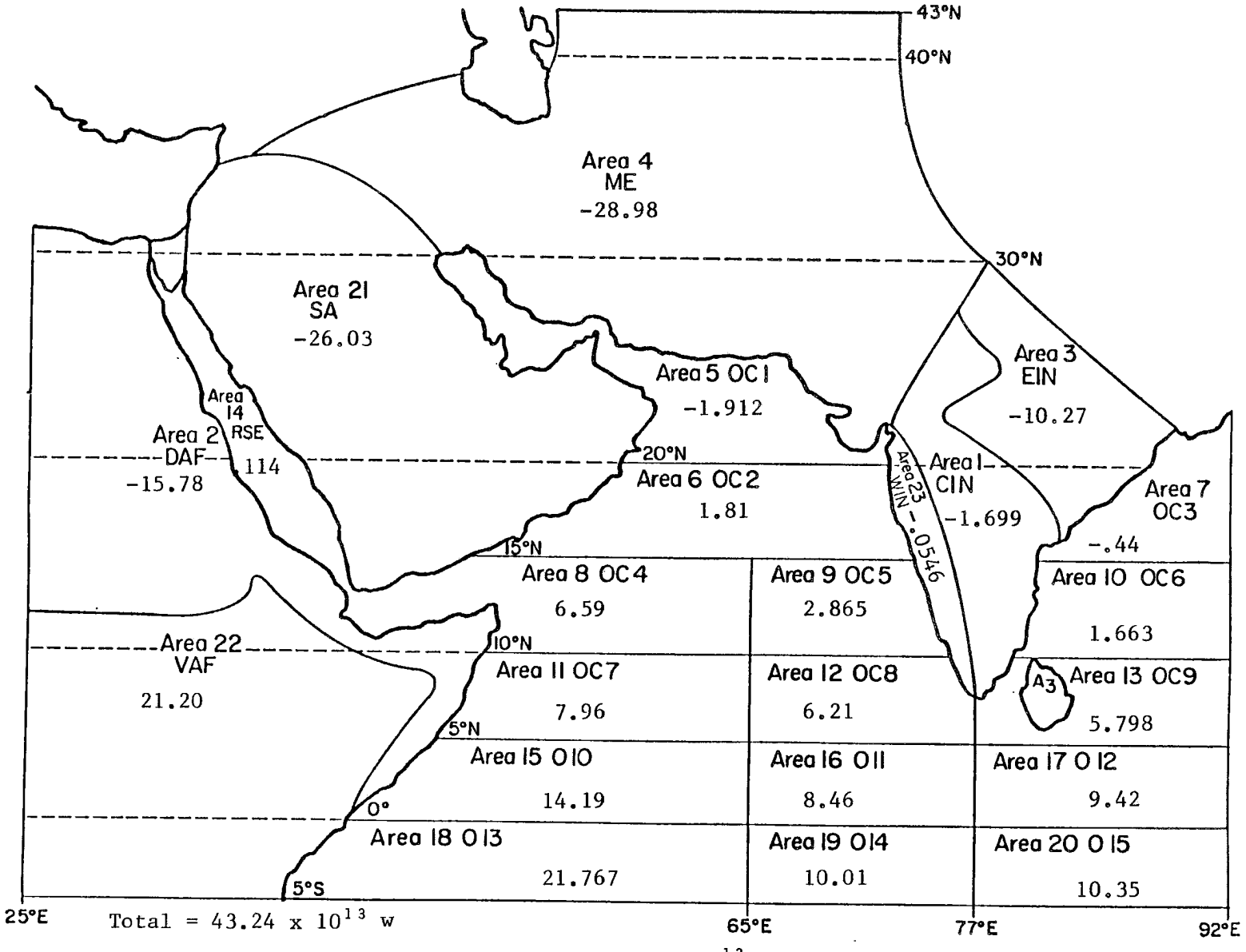

Figure 3.13 - January - Areal Net Radiation - w x 10^{13}

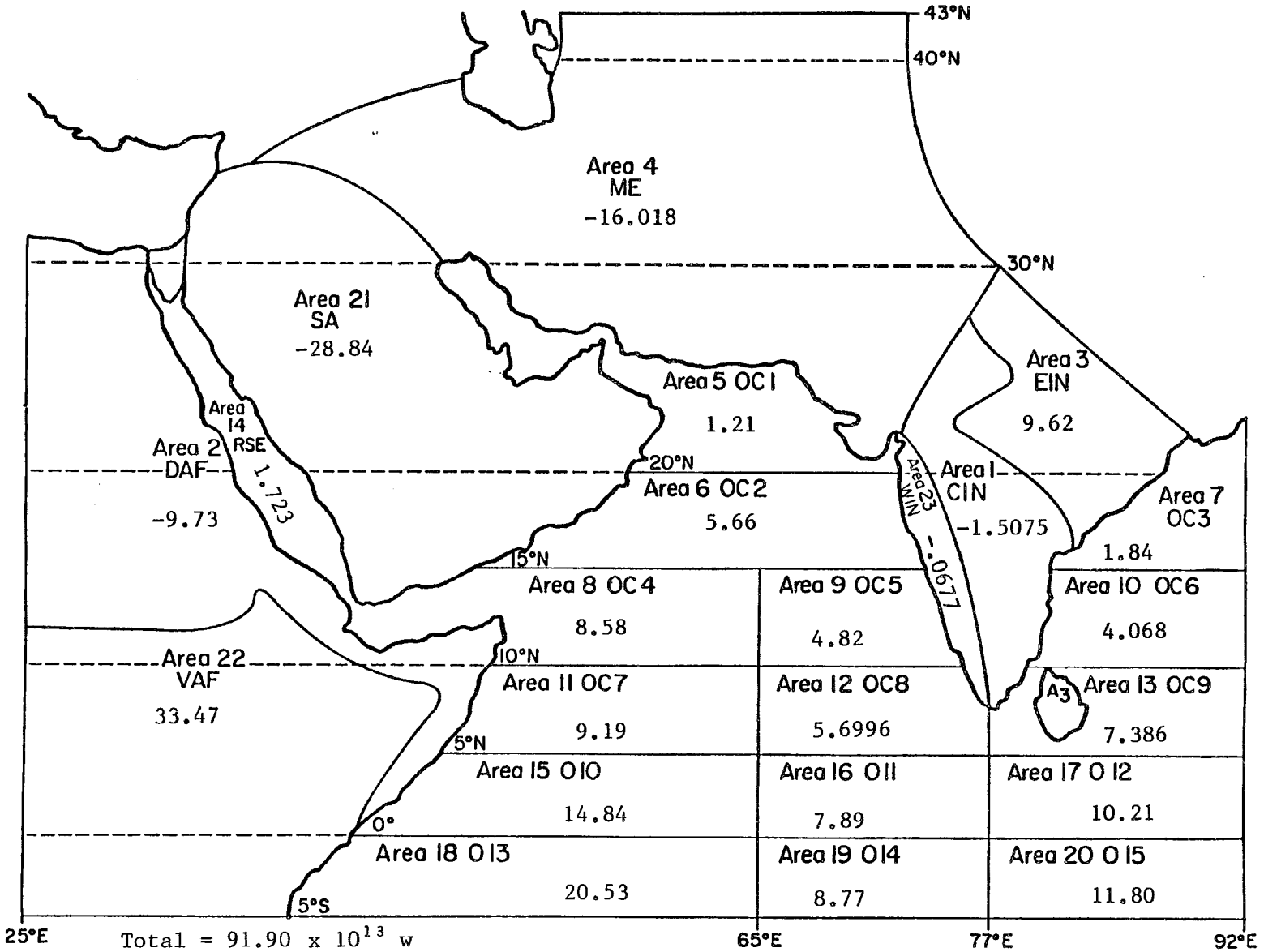

Total = 91.90 x 10^{13} w

Figure 3.14 - February - Areal Net Radiation - w x 10^{13}

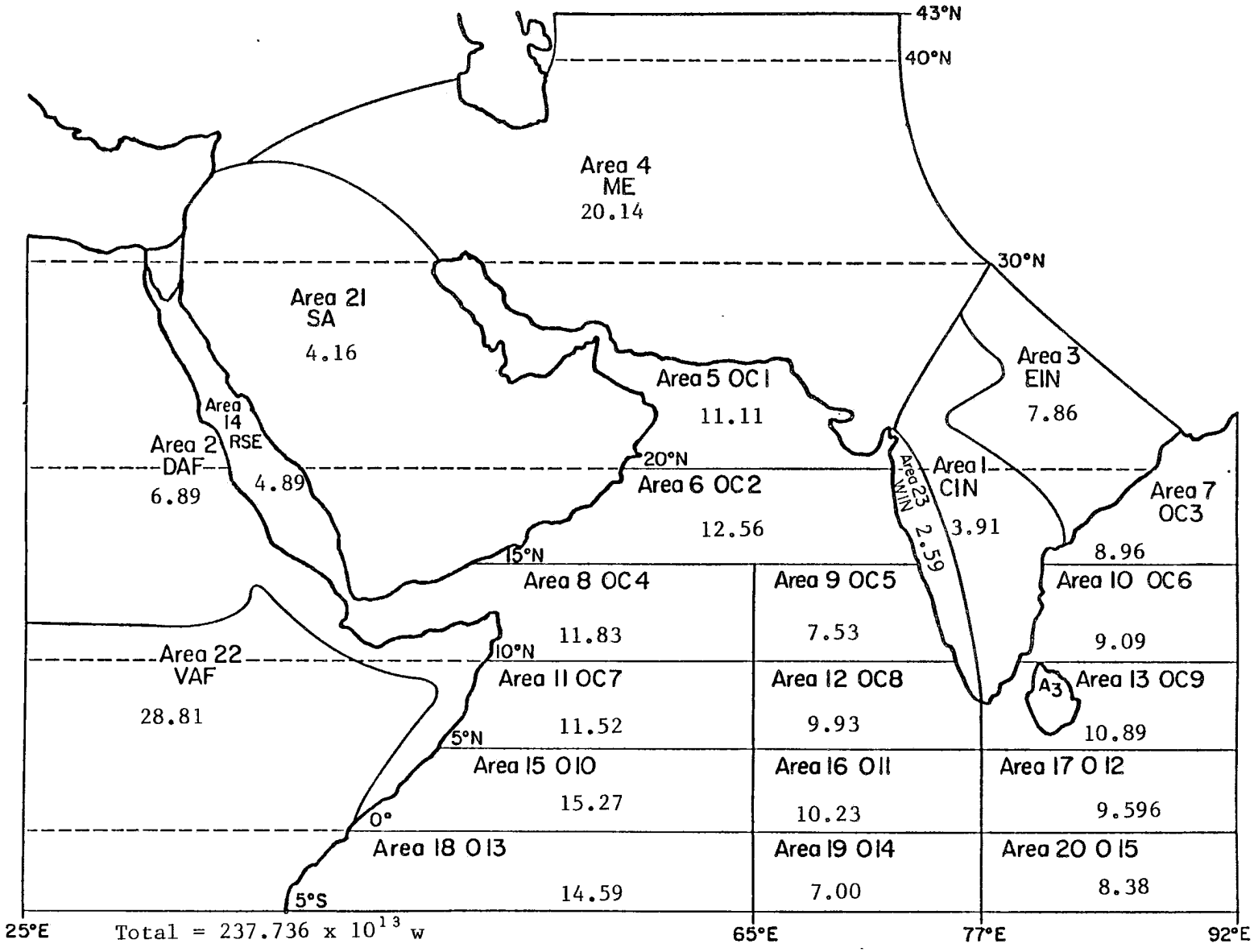

Figure 3.15 - May - Areal Net Radiation - w x 10^{13}

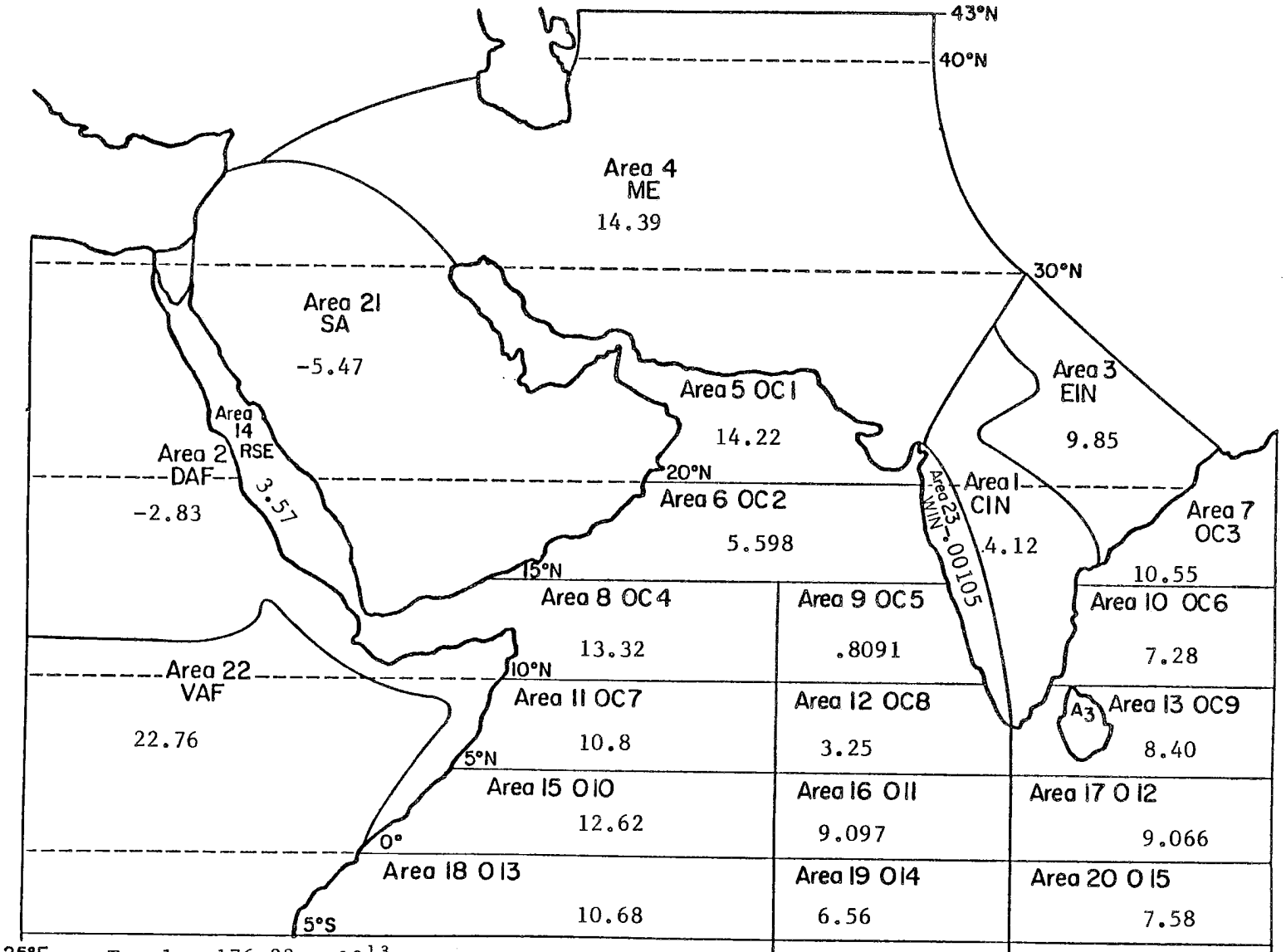

Total = 176.22 x 10^{13} w

Figure 3.16 - June - Areal Net Radiation - w x 10^{13}

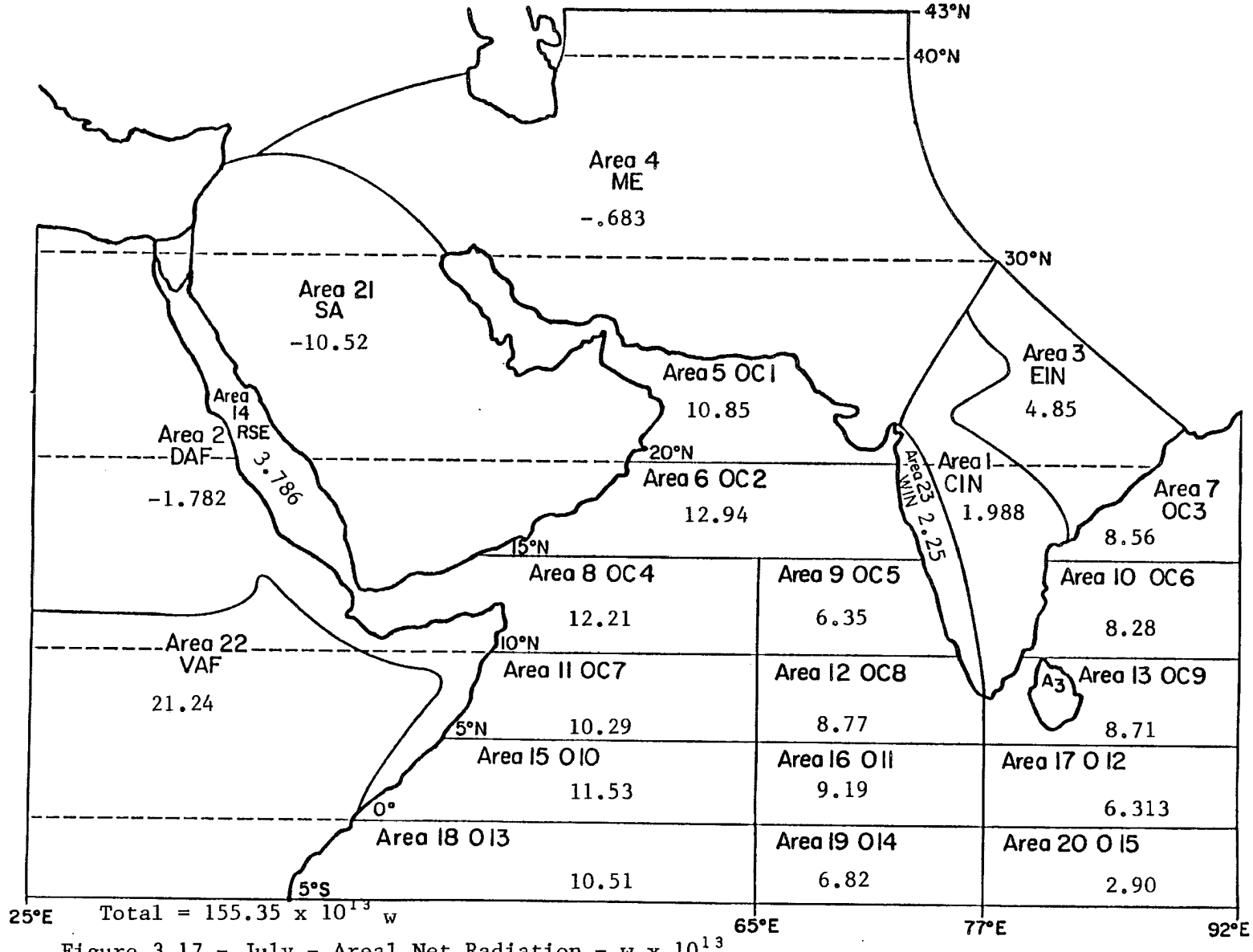

Total = 155.35×10^{13} w

Figure 3.17 - July - Areal Net Radiation - w x 10^{13}

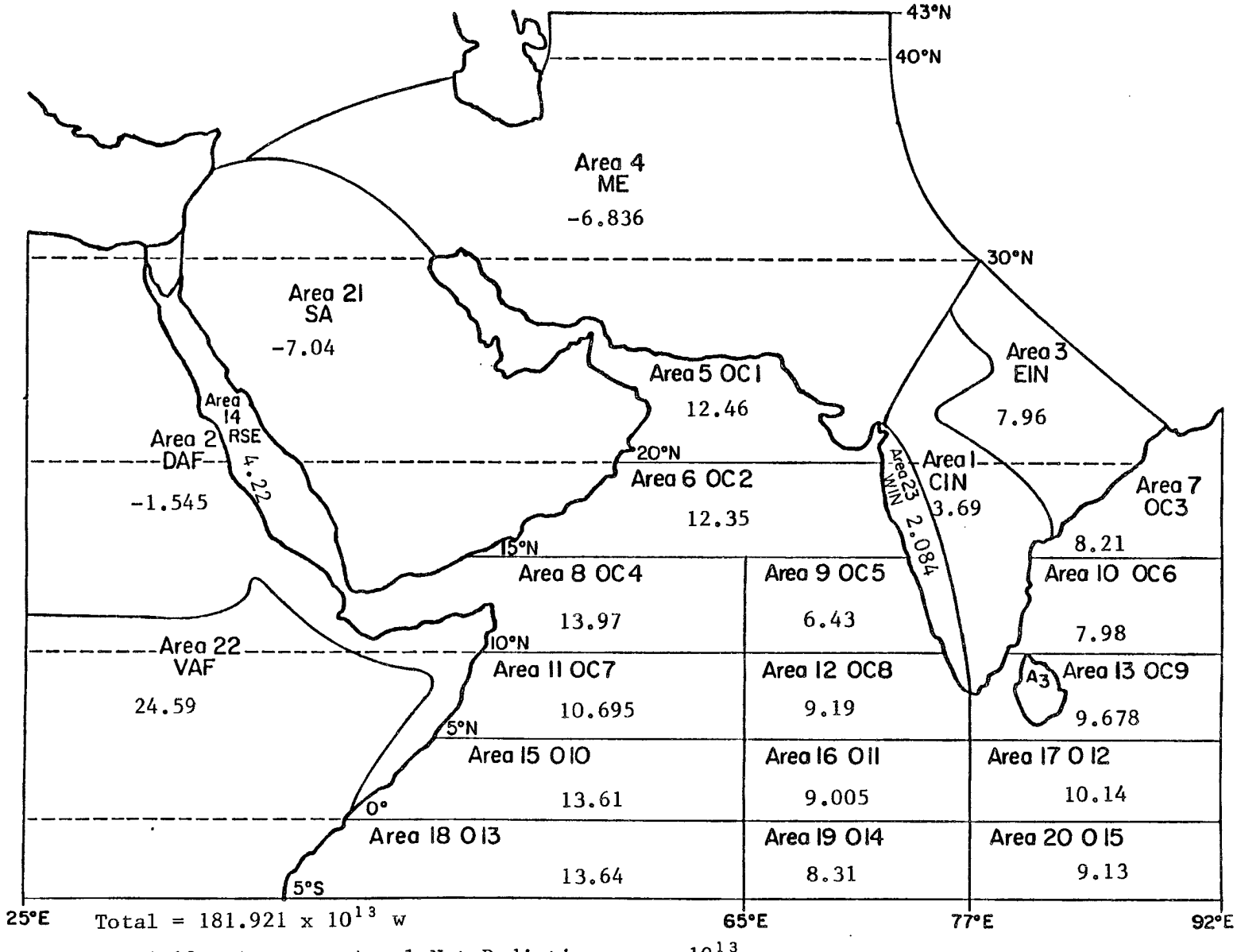

Figure 3.18 - August - Areal Net Radiation - w x 10^{13}

in total areal net radiation between the May and June data, a drop of 61.52 x 10^{13} w to the June value of 176.22 x 10^{13}. The July and August values recover some what from this drop, but never quite return to the May maximum.

III.B.2. Radiation Parameters of 1979 Compared to Previous Years

Winston and Krueger (1977) did a diagnostic radiation study of the Indian monsoon area using data gathered from NOAA polar orbiting satellites for the years 1974-1976. In comparison with their data set, 1979 had much less cloudiness than any of the other three years. For example, in May 1979 we have already noted the pronounced minimum in albedos over much of the MONEX region, with the exceptions being areas OC8 (#12), O11 (#16), O12 (#17), and O14 (#19) with albedos of .12, .11, .17, and .12, respectively.

In 1975, according to Winston and Krueger, there seemed to be much more general cloudiness over the Arabian Sea, with values for the albedos in the range of .20 to .30. Also the albedos in 1975 have higher values over WIN (#23) and CIN (#1). The only area with an albedo less than in 1979 is EIN (#3), while both sets of albedos agree on the values for SA (#21) and ME (#3).

In 1976, also considered to be a subnormal monsoon year (Winston and Krueger, 1977), as is 1979, there is a better correlation between the albedos of the data sets for May. Winston and Krueger's data show evidence of a persistent cloud band from 60° E to 79° E centered at 5° N. This is approximately the same area the cloud band appears at in this study, the major difference between the two studies being the magnitudes of the albedos. In 1976 the albedo values are greater than .20, while in 1979 they are between .11 and .17. Over the rest of the

study region, there is a rather striking similarity in albedo values, especially over the north Arabian Sea, where both studies have values below .10.

Also included in Winston and Krueger (1977) are maps of the outgoing LW radiation for June, July, and August of the years 1974-1976. In June 1974 the entire region has greater values of outgoing LW than in 1979, indicating that 1974 probably had even fewer clouds than 1979. June 1975 was in close agreement with 1979 over the land areas, but the Arabian Sea had higher values in 1975, again probably due to less cloud cover. In the other subnormal year, 1976, SA (#21) had higher values than 1979, along with the west coast area of India, which is a relative minimum of outgoing LW (cloud area) in both years. In 1979 the areal extent of this cloud cover was greater than in 1976. For the month of July, in 1974 the areas of ME (#3), SA (#21), and WIN (#23) all seem to be in near agreement with the values for 1979. EIN (#3) has values for 1974 that are less than 1979, and over the ocean areas southwest of the Indian peninsula there is more outgoing LW in 1974. These last two features also appear in a comparison of July 1975 data with July 1979. Also in 1975, the west Arabian Sea and the desert areas seem to have close to the same values for outgoing LW as in 1979. In 1976, as one might expect from two similar years, almost the entire region is in agreement with 1979 values. Exceptions to the general agreement are over the Bay of Bengal and the areas south to the edge of the study region, where 1979 must have been much cloudier, since the outgoing LW is less than 200 w/m^2. In 1976 the same area had values around 225 w/m^2.

The last month to be used in both studies was August. In 1974 the outgoing values are greater for the areas WIN (#23), CIN (#1), OC1 (#5), OC2 (#6), and OC3 (#7). EIN (#3) had less LW loss over the same period. The three ocean areas had similar values in 1975, again losing more energy to space than in 1979. The desert areas, along with EIN (#3) and the ocean areas off the east Indian coast, are all emitting about the same values as in 1979. August 1976 seems to be clearer over the deserts than 1979, since the LW loss is greater in 1976. The Indian Ocean south of the peninsula, especially over area #20, 015, also have a greater LW loss in 1976. However, EIN (#3), with less of a outgoing LW value in 1976, might have had a slightly longer monsoon season that year.

III.B.3. A Comparison of the Importance of Insolation and Albedo

The change in the SW component of the radiation balance equation may be decomposed into a change in the magnitude of the insolation (Q), and the change in the albedo.

$$\frac{\Delta SW}{SW} = \underset{(1)}{\frac{\Delta Q}{Q}} - \underset{(2)}{\frac{\Delta \alpha}{1-\alpha}} \qquad (3)$$

Table 3.4 shows a comparison of terms 1 and 2 for the study area. North of approximately 10° N, mainly due to the solar geometry, the percent change in Q dominates the SW for the periods January-February and February-May, while changes in albedo, except over the deserts and Africa, dominates the other three time periods, with the fluctuations in cloudiness an important factor. The importance of the solar geometry in Q and the cloud amounts in the albedo are the deciding factors in most all of the cases. ΔQ dominates when the sun is at

Table 3.4

$\frac{\Delta Q}{Q}$ compared to $\frac{\Delta \alpha}{1-\alpha}$ (% change)

Area	Jan.-Feb. Δδ	Jan.-Feb. Δα	Feb.-May Δδ	Feb.-May Δα	May-June Δδ	May-June Δα	June-July Δδ	June-July Δα	July-August Δδ	July-August Δα
1 CIN	11.1	2.7	17.2	-14.1	- .97	9.9	- .49	19.2	-2.97	-15.25
2 DAF	9.3	0	11.4	- 8.8	1.7	4.0	- .26	0	.41	1.4
3 EIN	15.8	1.5	32.7	-17.9	.67	7.6	-1.0	20.5	-3.2	-13.8
4 ME	23.1	7.6	55.7	-18.0	2.6	-2.8	-1.6	2.7	-6.15	1.4
5 OC1	16.6	-1.1	35.2	-3.3	.9	3.2	-1.1	8.9	-3.6	-6.1
6 OC2	11.4	-3.4	18.2	-2.2	- .85	32.3	- .52	-28.6	-.87	-2.5
7 OC3	11.4	-2.4	18.2	-2.4	- .85	6.9	- .52	7.4	-.87	0
8 OC4	8.5	-4.5	36.1	-1.1	-2.0	12.9	-1.4	- 9.9	.97	-3.4
9 OC5	8.5	-3.4	36.1	-2.2	-2.0	46.2	-1.4	-60	.97	-3.8
10 OC6	8.5	0	36.1	-7.1	-2.0	1.7	-1.4	- 2.7	.97	-3.9
11 OC7	5.98	-2.3	.2	-3.4	-3.2	8.8	.25	-9.7	2.9	0
12 OC8	5.98	7.8	.2	-6	-3.2	35.2	.25	-47.4	2.9	-1.2
13 OC9	5.98	1.2	.2	-5.9	-3.2	11.2	.25	- 1.3	2.9	-5.0
14 RSE	12.3	-2.2	21.3	2.2	- .5	2.2	-.64	0	-1.4	-2.3
15 010	3.7	2.2	-7.4	-4.5	-4.4	9.8	.66	- 8.4	4.9	0
16 011	3.7	6.6	-7.4	-4.7	-4.4	9.0	.66	- 8.6	4.9	6.8
17 012	3.7	5.8	-7.4	-2.5	-4.4	2.4	.66	8.6	4.9	-6.8
18 013	1.6	-1.1	-14.5	-2.2	-5.6	9.8	1.1	-6.0	7.0	-2.3
19 014	1.6	9.0	-14.5	-8.6	-5.6	6.8	1.1	-3.7	7.0	3.5
20 015	1.6	6.1	-14.5	-14.3	-5.6	6.8	1.1	18.3	7.0	-8.9
21 SA	13.67	-3.3	25.6	-9.5	- .04	0	-.79	1.45	-2.1	1.5
22 VAF	3.9	-1.3	-6.6	-3.8	-4.3	1.2	.62	0	4.65	2.5
23 WIN	.99	3.8	13.3	-9.2	-1.4	32.5	-.33	-19.6	.045	0

more oblique angles, and the change in albedo dominates when there are large changes in cloud amounts, or minimal changes in ΔQ. The latter two effects seem to happen concurrently in this area in the summer months. Closer to the equator the division of time periods into two separate blocks of dominance breaks down considerably, with variations with longitude introduced as well as the variations with latitude. Here the variations of Q aren't as great, so the effect of the clouds plays a larger role the year round.

III.C. A Note on the Influence Of Solar Zenith Angle on Ocean Albedo

The extreme influence of the solar zenith angles on the amount of energy reflected from water has been a noted fact for some time. Many previous studies, including Arking (1965), Brennan and Bandeen (1970), and Plass,et. al. (1975), have reported on this phenomenon. All have showed a major influence of solar zenith angle on the reflectance, and consequently the albedo, of an ocean surface. Since the albedo data for this study was taken at 11 GMT, some severe zenith angles were encountered in the course of the year, notably in the January data. For the purposes of this study, the cloud-free albedos for six areas, OC4-OC9 (areas #8-#13), from 15° N to 5° N, were examined for three different times of day (5, 7:30, and 11 GMT), and therefore for three different zenith angles. The day chosen was Julian Day 123, or May 3, because of the large range of zenith angles available from the data at hand. The total range of zenith angles ranged from 4.3° to 67.8° and the cloud-free albedos varied from .073 to .19. One interesting finding was that the largest zenith angle for an area was not always associated with the highest albedo. This happened in the

westernmost areas, OC4 (#8) and OC7 (#11), with zenith angles of 13.4° and 12.8° respectively, where sunglint was a factor. The sunglint also spilled slightly over to area OC5 (#9), where the smallest zenith angle, 4.3°, was the middle albedo value for that set. Other than these notable exceptions, the albedo increased with the zenith angle. A summary of the results can be seen in table 3.5.

Table 3.5

Effect of Solar Zenith Angle on Albedo

Area-OC4

Angle	Time	Albedo
13.3	7:30	.08
37.9	11:00	.07
49.5	5:00	.07

Area-OC5

Angle	Time	Albedo
4.3	7:30	.09
33.1	5:00	.09
54.3	11:00	.10

Area-OC6

Angle	Time	Albedo
17.2	7:30	.07
19.6	5:00	.08
67.7	11:00	.14

Area-OC7

Angle	Time	Albedo
12.8	7:30	.08
41.8	11:00	.07
47.6	5:00	.07

Area-OC8

Angle	Time	Albedo
8.4	7:30	.10
34.2	5:00	.11
55.3	11:00	.12

Area-OC9

Angle	Time	Albedo
17.9	7:30	.09
22	5:00	.10
67.8	11:00	.19

IV. CONCLUSIONS

The variation of albedo over 23 areas centered around the Arabian Sea has been studied and applied to a radiation budget. Six non-consecutive months from January to August 1979 were studied as part of the MONEX project. Data for this study were derived from images taken over the MONEX area by GOES-1 and Nimbus-7 satellites. The equations applied to the data were the result of work done by W. L. Smith, et. al. of the University of Wisconsin SSEC, 1981, where the flight track of the high altitude aircraft was superimposed over the GOES-1 satellite image at the corresponding time for a comparison of satellite data with in situ measurements. The resulting set of radiative balance equations were used in this study to derive total and cloud-free albedos that were then applied in conjunction with LW data from the Nimbus-7 ERB package to describe the net radiation over the study area. The albedos were averaged by month and separated into cloud-free and total albedos so that a comparison could be made between the two. It was a finding of this study that there was a pronounced minimum in albedo over most of the MONEX region in May. This was partially due to the lack of clouds in the area, however, since the cloud-free albedos also show this minimum, and show it in more areas, it may be supposed that the dominant effect is of the surface albedo changes. A related event shown by this study was a rise in the albedos of both types in the following month, June. The major cause for this change in the total albedos is the dramatic increase in the cloudiness

that accompanies the onset of the southwest monsoon. In response to the change in albedos in June, the net radiation of several areas to the west of, and including, the west Indian coast, exhibited a large decrease in net radiation in the June data as compared to the May data. This area of relative minimum values of net radiation, and relative maximums in albedo, moves east over the Indian peninsula in July, and remains there, although not as pronounced a feature, through August. This area of low values creates a strong E-W gradient in the radiational heating. Krishnamurti, et al., 1981 relates the dramatic increase in kinetic energy to differential heating in the monsoon region, although he looks to condensation as the principal source.

The most important result in the net radiation budget was for the month of May, a month with positive values over the entire study region. A major cause of this event is the aforementioned albedo minimum. Along with low values of outgoing LW radiation, and substantial incoming SW radiation, all three effects combine for enhanced radiative heating, creating a huge energy surplus that must be exported to achieve radiative balance. In fact, just considering radiation, and ignoring the considerable heat energy transferred by the monsoon rains, the months of June-September also show a large excess of net radiation averaged over the entire area. Some of the net radiation surpluses are quite large, up to 169 w/m^2 in area #8 (OC3; June). We have shown in the previous section that, generally speaking, the study area acts as a radiative heat source. If one totals the areal net radiation for the entire region, it is found that this is true for all of the months studied, with May having the greatest amount of surplus energy, 237.7×10^{13} w. It is interesting to note the drop in the

June value (176.2 x 10^{13} w), and the slow rise in July through August. It is likely that the condensational heating as a result of the monsoon helps make up some of the energy differences between the summer months.

This result leaves the question, where does this radiative surplus go? There are currently several theories that could be applied to this question. Pisharoty (1981) has conjectured that the monsoon is a "compensatory response of the ocean-atmosphere system of the Northern Hemisphere to an insufficent global poleward transport of energy across the latitude belt 30°N to 40°N during the immediately preceeding winter." To support his theory, he cites evidence linking snow cover over Tibet with the following summer's monsoon activity, and also showing the resulting magnitude of the poleward transport, compared to the measured values, as further proof.

Another theory looks at the Arabian Sea to utilize the excess energy (Raghavan, et. al., 1978). There is a dramatic change in the composition of the Arabian Sea over the monsoon period. Sea surface temperatures drop 2° to 3°C, and the depth of the mixed layer increases from 40-60m in May to 90-120m in July (Rao, et.al., 1981). However, no high pressure area forms over this relatively cool area. Perhaps the surplus radiation acts to supress this development by reducing the effects of the cold water being brought near the surface.

One last area that is a likely place for exported energy to go is over the Tibetan Plateau. Luo and Yanai (1983) have recently studied the heat and moisture budgets over the Plateau and surrounding areas. They conclude that the energy to support the giant circulatory feature known as the Tibetan High is generated differently over each half of

the Plateau. Over the eastern half, and including heating from deep convection over the Bay of Bengal, the major source of energy after the onset of the monsoon is condensational. Over the western half, however, the air is quite dry, and therefore the energy must come from the other major source, radiation, transported through the mechanism of dry convection.

This study was, an attempt to quantify the amount of excess radiation available for transport to any, or all of these regions. Further studies will be needed to get at the amounts needed by the particular area to be exported to, and if there is enough in radiation alone to totally satisfy all of the export demands, or if it is a combination of heat sources, as Luo and Yanai (1983) suggest in their work.

REFERENCES

Arking, A., 1965: The angular distribution of scattered solar radiation and the earth albedo as observed from TIROS. Goddard Institute for Space Studies, Annual Research Report, 1 July 1964-30 June 1965, 47-67.

Ackerman, S. and S. K. Cox, 1980: Colorado State University Radiation Instrumentation and Data Reduction Procedures for the CV-990 during Summer MONEX. Colorado State University, Atmospheric Science Paper No. 325, Fort Collins, CO.

Brennan, B., and W. R. Bandeen, 1970: Anisotropic reflectance characteristics of natural earth surfaces. Appl. Opt.,9, 405-412.

Bunker, Andrew F., 1968: Turbulence and Turbulent Fluxes over the Indian Ocean. Woods Hole Oceanographic Institute Technical Report 68-62, Woods Hole, Massachusetts. 30 pp.

Griffiths, J. F., Ed., 1972. Climates of Africa, Elsevier Publishing Co. Amsterdam, London, New York. Part of the World Survey of Climatology, Vol. 10.

Davis, J. M., and S. K. Cox, 1981: Regional properties of angular reflectance models. Colorado State University, Atmospheric Science Paper No. 338, Fort Collins, CO.

Ensor, G. J., 1978: User's Guide to the Operation of the NOAA Geostationary Satellite System. Technical Report, U.S. Department of Commerce, NOAA-NESS, Washington, D.C., 101 pp.

Fein, J. S., and J. P. Kuettner, 1980: Report on the summer MONEX field phase. Bull. of the Am. Met. Soc., 61, 461-474.

Flohn, H., 1968: Contributions to a Meteorology of the Tibetan Highlands. Colorado State University, Atmospheric Science Paper No. 130, Fort Collins, CO.

Global Atmospheric Research Program (GARP) WMO-ICSU Joint Organizing Committee, 1976: The Monsoon Experiment. GARP publication series no. 18.

Krishnamurti, T. N., and H. N. Bhalme, 1976: Oscillations of a monsoon system. Part 1. Observational aspects. Journal of the Atmospheric Sciences, 33, 1937-1954.

Krishnamurti, T. N., P. Ardanuy, Y. Ramanathan and R. Pasch, 1981: On the Onset Vortex of the Summer Monsoon. Monthly Weather Review, 109, 344-363.

Luo, Huibang and Michio Yanai, 1983: The Large-Scale Circulation and Heat Sources over the Tibetan Plateau and Surrounding Areas during the Early Summer of 1979. Part 1: Precipipation and Kinematic Analyses. Monthly Weather Review, 111, 922-944.

The Nimbus-7 User's Guide, edited by Charles R. Madrid, 1978. Technical Report, National Aeronautics and Space Administration, Goddard Space Center, Greenbelt, Maryland, 263 pp.

Miller, Albert, and Jack C. Thompson, 1975: Elements of Meteorology second edition, Charles E. Merrill Publishing Co., Columbus, Ohio.

Pisharoty, P. R., 1965: Evaporation from the Arabian Sea and the Indian southwest monsoon. Proc. Sym. Meteor. Results of .IIOE, 43-54.

Pisharoty, P. R., 1981: The Asiatic Summer Monsoon- A New Theory. International Conference on early results of FGGE. Tallahassee, FL.

Plass, G. N., G. W. Kattawar and J. A. Guinn Jr., 1975: Radiative transfer in the earth's atmosphere and ocean: influence of ocean waves. Appl. Opt., 14, 1924-1936.

Raghavan, K., P. V. Puranik, V. R. Mujumdar, P. M. M. Ismail and D. K. Paul, 1978: Interaction between the west Arabian Sea and the Indian monsoon. Monthly Weather Review, 106, 719-724.

Rao, R. R., P. G. K. Murty, M. G. Joseph, and K. V. S. Raman, 1981: On the space-time variability of ocean surface mixed layer characteristics of central and eastern Arabian Sea during monsoon-77. International Conference on the early results of FGGE. Tallahassee, FL.

Ramage,C.,1971: Monsoon Meteorology, Academic Press, New York. Part of the International Geophysics Series, Vol. 15, 296 pp.

Sellers, W., 1965: Physical Climatology, University of Chicago, Chicago, IL.

Smith, W. L., L. D. Herman, T. Schreiner, H. B. Howell and P. Menzel, 1981: Radiation budget characteristics of the onset of the summer monsoon. International Conference on early results of FGGE. Tallahassee, FL.

Trewartha and Horn, 1980: An Introduction to Climate, 5th edition, McGraw-Hill, New York.

Winston, J. S.,1971: The Annual Course of Zonal Mean Albedo as Derived from ESSA 3 and ESSA 5 Digitized Picture Data. Monthly Weather Review, 99, 818-827.

Winston, J. S. and Arthur F. Krueger, 1977: Diagnosis of the Satellite-Observed Radiative Heating in Relation to the Summer Monsoon. Pageoph, 115, 1131-1144.

APPENDIX A

Appendix A

Month:	Julian Day Used	Time of Image
January	013	11:00 GMT
	014	11:00 GMT
	015	11:00 GMT
	016	11:00 GMT
	017	11:00 GMT
	019	11:30 GMT
	020	11:00 GMT
February	042	11:00 GMT
	044	11:00 GMT
	045	11:00 GMT
	046	11:00 GMT
	047	11:00 GMT
May	136	11:00 GMT
	137	11:00 GMT
	138	11:00 GMT
	139	11:00 GMT
	140	11:00 GMT
	141	11:00 GMT
	142	11:00 GMT
June	166	11:00 GMT
	167	11:00 GMT
	168	11:00 GMT
	169	11:00 GMT
	170	11:00 GMT
	172	11:00 GMT
	173	11:00 GMT
July	197	11:00 GMT
	198	11:00 GMT
	199	11:00 GMT
	200	11:00 GMT
	201	11:00 GMT
	202	11:00 GMT
	203	11:00 GMT
August	225	11:00 GMT
	226	11:00 GMT
	227	11:30 GMT
	228	11:00 GMT
	229	11:00 GMT
	230	11:30 GMT
	231	11:00 GMT

BIBLIOGRAPHIC DATA SHEET	1. Report No.	2.	3. Recipient's Accession No.
4. Title and Subtitle Radiation Budget over the Indian Monsoon Region			5. Report Date February, 1984 6.
7. Author(s) Tracy Lorraine Smith and Stephen K. Cox			8. Performing Organization Rept. No. 376
9. Performing Organization Name and Address Department of Atmospheric Science Colorado State University Fort Collins, CO 80523			10. Project/Task/Work Unit No. 11. Contract/Grant No. ATM-8010691
12. Sponsoring Organization Name and Address National Science Foundation			13. Type of Report & Period Covered 14.

15. Supplementary Notes

16. Abstracts

A top of the atmosphere radiation budget is calculated over the Indian monsoon region for January, February, May, June, July and August of 1979. Albedos were inferred for 23 surface-type areas using GOES-1 satellite data. The longwave radiation values used in the budgets were monthly averages derived from the Nimbus-7 ERB experiment.

A regional minimum in albedo was found for the month of May, with a corresponding rise in albedo in June. The net radiation for May exhibited a positive (surplus) net radiation values over the entire study area, including the deserts. In June, a small region of local minimum values of net radiation developed over the west Indian coast and adjacent ocean areas. This area of relative low net values moved over the Indian subcontinent in July, and persisted through August. The study region as a whole was found to be a net radiative source region. Comparisons with previous studies show good correlation between the subnormal monsoon year of 1976 and the study year, 1979, also considered to be subnormal in terms of precipitation amounts.

17. Key Words and Document Analysis. 17a. Descriptors

17b. Identifiers/Open-Ended Terms

17c. COSATI Field/Group

18. Availability Statement	19. Security Class (This Report) UNCLASSIFIED	21. No. of Pages 64
	20. Security Class (This Page) UNCLASSIFIED	22. Price

FORM NTIS-35 (Rev. 3-72)